Astronomy & Astrophysics

Pulsating low-mass white dwarfs in the frame of new evolutionary sequences

V. Asteroseismology of ELMV white dwarf stars

Leila M. Calcaferro[1,2], Alejandro H. Córsico[1,2], and Leandro G. Althaus[1,2]

[1] Grupo de Evolución Estelar y Pulsaciones, Facultad de Ciencias Astronómicas y Geofísicas, Universidad Nacional de La Plata, Paseo del Bosque s/n, 1900 La Plata, Argentina
e-mail: [lcalcaferro;acorsico;althaus]@fcaglp.unlp.edu.ar

[2] Instituto de Astrofísica La Plata, CONICET-UNLP, Paseo del Bosque s/n, 1900 La Plata, Argentina

ABSTRACT

Context. Many pulsating low-mass white dwarf stars have been detected in the past years in the field of our Galaxy. Some of them exhibit multiperiodic brightness variation, therefore it is possible to probe their interiors through asteroseismology.

Aims. We present a detailed asteroseismological study of all the known low-mass variable white dwarf stars based on a complete set of fully evolutionary models that are representative of low-mass He-core white dwarf stars.

Methods. We employed adiabatic radial and nonradial pulsation periods for low-mass white dwarf models with stellar masses ranging from 0.1554 to 0.4352 $M_\odot$ that were derived by simulating the nonconservative evolution of a binary system consisting of an initially 1 $M_\odot$ zero-age main-sequence (ZAMS) star and a 1.4 $M_\odot$ neutron star companion. We estimated the mean period spacing for the stars under study (where this was possible), and then we constrained the stellar mass by comparing the observed period spacing with the average of the computed period spacings for our grid of models. We also employed the individual observed periods of every known pulsating low-mass white dwarf star to search for a representative seismological model.

Results. We found that even though the stars under analysis exhibit few periods and the period fits show multiplicity of solutions, it is possible to find seismological models whose mass and effective temperature are in agreement with the values given by spectroscopy for most of the cases. Unfortunately, we were not able to constrain the stellar masses by employing the observed period spacing because, in general, only few periods are exhibited by these stars. In the two cases where we were able to extract the period spacing from the set of observed periods, this method led to stellar mass values that were substantially higher than expected for this type of stars.

Conclusions. The results presented in this work show the need for further photometric searches, on the one hand, and that some improvements of the theoretical models are required on the other hand in order to place the asteroseismological results on a firmer ground.

Key words. stars: evolution – stars: interiors – stars: oscillations – white dwarfs

1. Introduction

White dwarf (WD) stars are the last stage in the life of the majority of stars (Winget & Kepler 2008; Fontaine & Brassard 2008; Althaus et al. 2010). Most WDs have envelopes rich in H, and they define the spectral class DA WD, whose distribution peaks at 0.59 $M_\odot$. This class also shows a peak at low mass: $M_\star/M_\odot \lesssim 0.45$. These stars are thought to be the result of strong mass-loss episodes in interactive binary systems before the He flash during the red giant branch phase of low-mass stars (Althaus et al. 2013; Istrate et al. 2016b, for recent studies). At variance with average WDs with C and O cores, they are expected to contain He cores, since He burning is avoided. Specifically, this interactive binary evolutionary scenario is thought to be the most plausible origin for the so-called extremely low-mass (ELM) WDs, which have masses below ∼0.18−0.20 $M_\odot$.

In the past years, numerous low-mass WDs, including ELM WDs, have been discovered via the ELM survey and the SPY and WASP surveys (see Koester et al. 2009; Brown et al. 2010, 2012, 2013; Maxted et al. 2011; Kilic et al. 2011, 2012, 2015; Giannnas et al. 2014a, 2015). The detection of pulsation

g modes (gravity modes) in some of them (Hermes et al. 2012, 2013b,a; Kilic et al. 2015; Bell et al. 2015, 2017) has given rise to a new class of variable WDs, the ELMVs. These pulsating low-mass WDs provide us an exceptional chance for probing the interiors of these stars and possibly to test their formation scenarios by employing the tools of astero-seismology. Since g modes in ELMVs are restricted mainly to the core regions (Steinfadt et al. 2010; Córsico et al. 2012b; Córsico & Althaus 2014a), we would be able to constrain their core chemical structure. Furthermore, as shown by stability computations (Córsico et al. 2012b; Van Grootel et al. 2013; Córsico & Althaus 2016), a combination of the $\kappa - \gamma$ mechanism (Unno et al. 1989) and the "convective driving" mechanism (Brickhill 1991), both acting at the H-ionization region, excite long-period g modes, in agreement with observations. Moreover, some unstable short-period g modes could be driven by the ε mechanism as a result of stable H burning (Córsico & Althaus 2014b).

In addition to ELM stars, several objects are considered as their precursors, the so-called pre-ELMs. These stars

exhibit metals in their atmospheres (e.g., Gianninas et al. 2014b; Hermes et al. 2014; Istrate et al. 2016b). Interestingly enough, pulsations in a number of objects have been detected in the past years (Maxted et al. 2013, 2014; Zhang et al. 2016; Gianninas et al. 2016; Corti et al. 2016). Evolutionary models that consider only element diffusion cannot explain these properties (e.g., Córsico et al. 2016; Istrate et al. 2016a) and might be an indication that the missing physics might also affect the evolution of the objects on the cooling track (e.g., the thickness of the H envelope). Moreover, there are indications that a pre-ELMV WD will later be observed as an ELMV (Fontaine et al. 2017).

The definition of an ELM WD is still under debate. In the context of the ELM survey, an ELM WD is defined as an object with surface gravity of $5 \lesssim \log(g) \lesssim 7$ and effective temperature in the range of $8000 \lesssim T_{\mathrm{eff}} \lesssim 22\,000$ (e.g., Brown et al. 2010; Kilic et al. 2011; Brown et al. 2016). In addition, an ELM WD should be part of a tight binary system and therefore show short-period or high-amplitude velocity variability (e.g., Brown et al. 2017). Córsico & Althaus (2014a) suggested defining an ELM WD as a WD resulting from a progenitor star that did not undergo H-shell flashes as the pulsational properties are quite different from those of systems that experienced flashes. However, this mass limit depends on the metallicity of the progenitor stars (Istrate et al. 2016b).

White dwarf asteroseismology has already proven to be a very useful technique for peering into the interior of several pulsating WDs, and it has been applied by employing two different methods: one method considers stellar models with parametrized chemical composition profiles, and the other involves fully evolutionary models characterized by a consistent chemical structure. The former has the advantage of allowing a full exploration of the parameter space (the total mass, the mass of the H envelope, and the chemical composition of the core, among others) to find an optimal asteroseismological model. Examples of this approach are the pioneer works by Bradley (1998, 2001). More recent works using this avenue are from Pech et al. (2006), Pech & Vauclair (2006), Bischoff-Kim et al. (2008), Castanheira & Kepler (2008, 2009), Paparó et al. (2013), Bognár et al. (2016) and the recent developments of the core parameterization by Giammichele et al. (2016, 2017a,b). The second approach, developed at La Plata Observatory, is different but complementary, as it employs fully evolutionary models that are the result of the complete evolution of the progenitor stars, from the zero-age main sequence (ZAMS) until the WD phase. Examples of the application of this method to GW Virginis stars (pulsating PG1159 stars) are the works by Córsico et al. (2007a,b, 2008, 2009), Kepler et al. (2014) and Calcaferro et al. (2016). The method has also been applied in DBV WDs (He-rich atmosphere) by Córsico et al. (2012a) and Bognár et al. (2014). In ZZ Ceti stars, this approach has been successfully employed by Kepler et al. (2012) and Romero et al. (2012, 2013). In particular, this method has the added advantage that the chemical structure of the background models is consistent with the pre-WD evolution.

Here, we apply our asteroseismological approach for the first time to the complete set of the known ELMVs, whose spectroscopic parameters we describe in Table 1, and whose periods are listed in Tables 2 to 10, along with the corresponding frequencies and amplitudes. SDSS J184037.78+642312.3 (hereafter J1840) is the ELMV that was discovered first (Hermes et al. 2012, 2013a). SDSS J111215.82+111745.0 (hereafter J1112) was reported by Hermes et al. (2013b). This case is particularly interesting because this star shows seven periods, two

of which are very short, probably associated with p modes or radial modes. SDSS J151826.68+065813.2 (hereafter J1518) is the hottest ELMV so far, according to Hermes et al. (2013b). This star shows seven independent periods, which makes a more detailed asteroseismological analysis possible. SDSS J161431.28+191219.4 (hereafter J1614) is an ELMV, according to Hermes et al. (2013a). SDSS J222859.93+362359.6 (hereafter J2228) is the coolest EMLV known to date, according to Hermes et al. (2013a). This star exhibits only three independent periods in the range $\sim[3255-6235]$ s, so these periods seem to be approximately in the asymptotic regime (see Córsico & Althaus 2014a). In particular, the period 6234.9 s is the longest period ever measured in a pulsating WD star. PSR J1738+0333 is a millisecond pulsar that has an ELMV companion (which we call J1738 for short), according to Kilic et al. (2015). This case is particularly interesting because it is the only binary system with a millisecond pulsar and a pulsating WD. SDSS J161831.69+385415.15 (hereafter J1618) is an ELMV, according to Bell et al. (2015). Finally, SDSS J1735+2134 (hereafter J1735) and SDSS J2139+2227 (hereafter J2139) are two recently detected ELMVs, according to Bell et al. (2017). In particular, the former has very long periods, which seem to be in the asymptotic regime of nonradial g modes (see Córsico & Althaus 2014a). It is worth mentioning how the spectroscopic masses of the ELM WDs are determined. Brown et al. (2017) showed that for the same metallicity of the progenitor stars there is a 15% difference in the mass of ELM WDs for the same $\log(g)$ and T_{eff} parameters, using either the Althaus et al. (2013) evolutionary tracks or the Istrate et al. (2016b) evolutionary tracks. We can adopt this difference as the true uncertainty in the spectroscopic determination of the masses of ELM WDs. In Fig. 1 we show the location of the different families of pulsating WDs, including all the known ELMV stars (red circles). The total number of ELMVs rises to nine because there is a high probability that the star discovered by Bell et al. (2017), SDSS J1355+1956, is a δ Scuti pulsator, as claimed by these authors. In this sense, it is important to stress here that some of the stars under analysis in this work may not be pulsating ELM WDs. The analysis reported by Brown et al. (2017) suggests that there are only four pulsating ELM WDs: J1840, J1112, J1518, and J1738. In addition, as discussed by Bell et al. (2015, 2017), the stars J1618, J1735, and J2139 may not be ELM WD stars. A measurement of the rate of period change for these stars could help to shed light on this question (Calcaferro et al. 2017). Despite this, given the exploratory nature of this work, we consider that these stars are genuine ELMVs and they are included in our analysis.

In this paper we report a further step in the study of low-mass WD stars by performing an asteroseismological analysis of all the known ELMVs. This is the fifth work of a series dedicated to these stars. The first paper (Córsico & Althaus 2014a) was focused on the adiabatic properties of these stars; the second paper (Córsico & Althaus 2016) was dedicated to the nonadiabatic pulsation stability features of these stars. The third work (Córsico et al. 2016) was aimed at studying the pulsation properties of the pre-ELMV WDs. The fourth paper (Calcaferro et al. 2017) was focused on studying the theoretical temporal rates of the period change of ELMV and pre-ELMV stars. In this work, we follow the asteroseismological approach that employs fully evolutionary models resulting from the complete evolution of the progenitor stars. The employment of fully evolutionary models is a crucial requirement because some models (particularly those with the lowest mass) are characterized by strong H-nuclear burning that depends sensitively on the

Table 1. Stellar parameters (derived using 1D and 3D model atmospheres) and observed pulsation properties of all the known ELMV WD stars.

Star	$T_{\rm eff}^{\rm 1D}$	$\log(g)^{\rm 1D}$	$M_\star^{\rm (1D)}$	$T_{\rm eff}^{\rm 3D}$	$\log(g)^{\rm 3D}$	$M_\star^{\rm (3D)}$	Period range
	[K]	[cgs]	$[M_\odot]$	[K]	[cgs]	$[M_\odot]$	[s]
J1840	9390 ± 140	6.49 ± 0.06	$0.183^{a,b}$	9120 ± 140	6.34 ± 0.05	0.177^c	[1164–4445]
J1112	9590 ± 140	6.36 ± 0.06	0.179^d	9240 ± 140	6.17 ± 0.06	0.169^c	[108–2856]
J1518	9900 ± 140	6.80 ± 0.05	0.220^d	9650 ± 140	6.68 ± 0.05	0.197^c	[1335–3848]
J1614	8800 ± 170	6.66 ± 0.14	0.192^b	8700 ± 170	6.32 ± 0.13	0.172^c	[1184–1263]
J2228	7870 ± 120	6.03 ± 0.08	0.152^b	7890 ± 120	5.78 ± 0.08	0.142^c	[3255–6235]
J1738	9130 ± 140	6.55 ± 0.06	0.181^e	8910 ± 150	6.30 ± 0.10	0.172^c	[1788–3057]
J1618	9144 ± 120	6.83 ± 0.14	0.220^f	8965 ± 120	6.54 ± 0.14	0.179^c	[2543–6126]
J1735	–	–	–	7940 ± 130	5.76 ± 0.08	0.142^g	[3363–4961]
J2139	–	–	–	7990 ± 130	5.93 ± 0.12	0.149^g	[2119–3303]

References. [a] Hermes et al. (2012). [b] Hermes et al. (2013a). [c] Determined using the corrections for 3D effects by Tremblay et al. (2015). [d] Hermes et al. (2013b). [e] Kilic et al. (2015). [f] Bell et al. (2015). [g] Bell et al. (2017).

Table 2. The five independent frequencies in the data of J1840 from Hermes et al. (2012).

Π [s]	Freq. [μHz]	Ampl. [mmag]
1164.15 ± 0.38	859.0 ± 0.29	1.78 ± 0.29
1578.7 ± 0.65	633.43 ± 0.26	2.831 ± 0.41
2376.07 ± 0.74	420.86 ± 0.13	4.817 ± 0.46
3930.0 ± 300	254.0 ± 19	2.7 ± 2.0
4445.3 ± 2.4	224.96 ± 0.12	7.6 ± 1.6

Table 3. The seven independent frequencies in the data of J1112 from Hermes et al. (2013b).

Π [s]	Freq. [μHz]	Ampl. [mmag]
107.56 ± 0.04	9297.4 ± 3.6	0.38 ± 0.14
134.275 ± 0.001	7447.388 ± 0.0100	0.44 ± 0.08
1792.905 ± 0.005	557.7542 ± 0.0017	3.31 ± 0.08
1884.599 ± 0.004	530.6170 ± 0.0011	4.73 ± 0.08
2258.528 ± 0.003	442.7662 ± 0.0007	7.49 ± 0.08
2539.695 ± 0.005	393.7480 ± 0.0007	6.77 ± 0.09
2855.728 ± 0.010	350.1734 ± 0.0013	3.63 ± 0.09

Table 4. The seven independent frequencies in the data of J1518 from Hermes et al. (2013b).

Π [s]	Freq. [μHz]	Ampl. [mmag]
$1335,318 \pm 0.003$	748.8855 ± 0.0015	13.6 ± 0.6
$1956,361 \pm 0.003$	511.1532 ± 0.0007	18.1 ± 0.3
$2134,027 \pm 0.004$	468.5976 ± 0.0008	14.2 ± 0.4
$2268,203 \pm 0.004$	440.8777 ± 0.0007	21.6 ± 0.2
$2714,306 \pm 0.003$	368.4183 ± 0.0005	21.6 ± 0.9
2799.087 ± 0.005	357.2593 ± 0.0007	35.4 ± 0.6
3848.201 ± 0.009	259.8617 ± 0.0006	15.7 ± 0.3

Table 5. The two independent frequencies in the data of J1614 from Hermes et al. (2013a).

Π [s]	Freq. [μHz]	Ampl. [mmag]
1184.106 ± 0.064	844.519 ± 0.045	3.20 ± 0.10
1262.668 ± 0.041	791.974 ± 0.026	5.94 ± 0.11

Table 6. The three independent frequencies in the data of J2228 from Hermes et al. (2013a).

Π [s]	Freq. [μHz]	Ampl. [mmag]
3254.5 ± 2.1	307.27 ± 0.20	2.34 ± 0.14
4178.3 ± 2.8	239.33 ± 0.16	6.26 ± 0.14
6234.9 ± 6.0	160.39 ± 0.15	1.94 ± 0.23

Table 7. The three independent frequencies in the data of J1738 from Kilic et al. (2015).

Π [s]	Freq. [μHz]	Ampl. [mmag]
1788 ± 33	559 ± 10	1.27 ± 0.47
2656 ± 80	376 ± 11	1.15 ± 0.47
3057 ± 99	327 ± 11	1.22 ± 0.47

Table 8. The three independent frequencies in the data of J1618 from Bell et al. (2015).

Π [s]	Freq. [μHz]	Ampl. [mmag]
2543.0 ± 10	393.2 ± 1.6	16 ± 3
4935.21 ± 0.07	202.605 ± 0.003	56.3 ± 1.3
6125.9 ± 0.2	163.240 ± 0.006	25.5 ± 1.4

thickness of the H envelope, a quantity that results from the previous evolution. We employ the adiabatic radial ($\ell = 0$) and nonradial ($\ell = 1, 2$) p- and g-mode pulsation periods computed in Córsico & Althaus (2014a) on low-mass He-core WD evolutionary models with stellar masses ranging from 0.1554 to 0.4352 $M_\odot$, extracted from the computations of Althaus et al. (2013), which take the binary evolution of the progenitor stars into account.

The paper is organized as follows. A brief summary of the stellar models and the pulsational code employed is provided in Sect. 2. In Sect. 3 we describe the asteroseismological analyses we carried out. Next, in Sect. 3.1, we try to determine (when possible) the observed period spacing for the target stars, and then in Sect. 3.2 we constrain the stellar mass by comparing the observed period spacing with the average of the computed period spacings. In Sect. 3.3 we search for the best-fit asteroseismological model by comparing the individual periods from each ELMV star with theoretical periods from our grid of models. Finally, in Sect. 4 we summarize the main findings of this work.
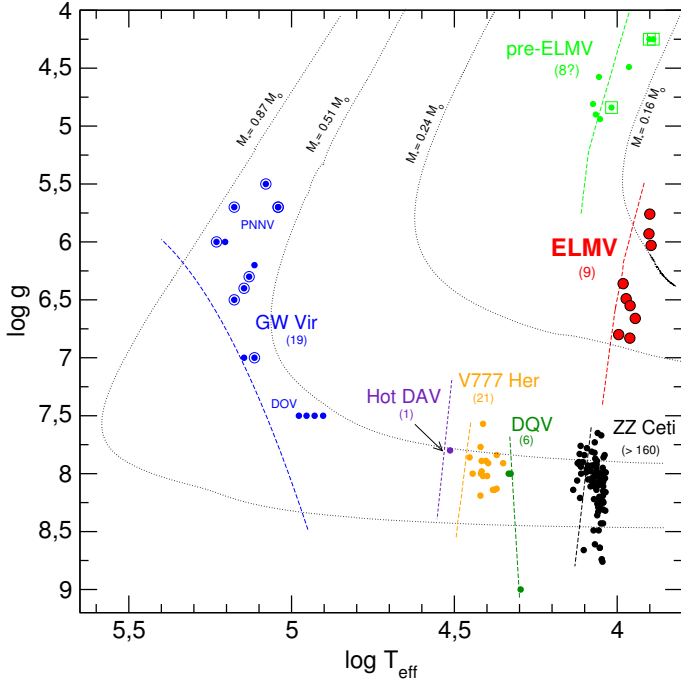
Fig. 1. Location of the known ELMVs (red circles) along with the other classes of pulsating WD stars (dots of different colors) in the $\log T_{\rm eff} - \log g$ plane. The nature of the three stars emphasized with squares surrounding the light green circles is currently unclear (they could be pre-ELMV stars as well as SX Phe and/or δ Scuti stars). In parenthesis we include the number of known members of each class. Two post-VLTP evolutionary tracks for H-deficient WDs and two evolutionary tracks for low-mass He-core WDs are plotted for reference. Dashed lines indicate the theoretical blue edge for the different classes of pulsating WDs.

Table 9. The four independent frequencies in the data of J1735 from Bell et al. (2017).

Π [s]	Freq. [μHz]	Ampl. [mmag]
3362.76 ± 0.54	297.38 ± 0.05	2.04 ± 0.11
3834.54 ± 0.42	260.79 ± 0.03	3.64 ± 0.11
4541.88 ± 0.24	220.172 ± 0.013	7.60 ± 0.11
4961.22 ± 0.72	201.56 ± 0.03	3.38 ± 0.11

Table 10. The three independent frequencies in the data of J2139 from Bell et al. (2017).

Π [s]	Freq. [μHz]	Ampl. [mmag]
2119.44 ± 0.24	471.82 ± 0.06	1.52 ± 0.08
2482.32 ± 0.54	402.85 ± 0.09	1.02 ± 0.08
3303.30 ± 0.96	302.73 ± 0.09	0.99 ± 0.08

2. Evolutionary models and pulsational code

In this work, we have employed the fully evolutionary models of low-mass He-core WDs generated with the LPCODE stellar evolution code. This code computes in detail the complete evolutionary stages that lead to the WD formation, allowing the study of the WD evolution consistently with the predictions of the evolutionary history of progenitors. Details of the LPCODE can be found in Althaus et al. (2005, 2009, 2013, 2015) and references therein. Here, we briefly mention the ingredients employed that are relevant for our analysis of low-mass He-core

WD (see Althaus et al. 2013, for details). The standard mixing length theory (MLT) for convection in the ML2 prescription is used (see Tassoul et al. 1990, for its definition), but adiabatic periods do not sensitively depend on the specific version of the MLT convection theory that is employed (Bradley 1998). We assumed the metallicity of the progenitor stars to be $Z = 0.01$. We considered the radiative opacities for arbitrary metallicity in the range of 0 to 0.1 from the OPAL project (Iglesias & Rogers 1996). Conductive opacities are those of Cassisi et al. (2007). For the main-sequence evolution, we considered the equation of state from OPAL for H- and He-rich compositions. We also adopted from Itoh et al. (1996) the neutrino emission rates for pair, photo, and bremsstrahlung processes, and for plasma processes, we included the treatment of Haft et al. (1994). For the WD regime we have employed an updated version of the equation of state of Magni & Mazzitelli (1979). The nuclear network takes into account 16 elements and 34 thermonuclear reaction rates for pp-chains, CNO bi-cycle, He burning, and C ignition. We also considered time-dependent diffusion due to gravitational settling and chemical and thermal diffusion of nuclear species following the multicomponent gas treatment of Burgers (1969). We have computed abundance changes according to element diffusion, nuclear reactions, and convective mixing, a treatment that represents a very significant aspect in evaluating the importance of residual nuclear burning during the cooling stage of low-mass WDs.

The pulsation analysis was carried out for radial ($\ell = 0$) and nonradial ($\ell = 1, 2$) p and g modes, on the basis of the set of adiabatic and nonadiabatic pulsation periods presented in Córsico & Althaus (2014a, 2016), computed employing the adiabatic and nonadiabatic versions of the LP-PUL pulsation code (Córsico & Althaus 2006; Córsico et al. 2006). The adiabatic version of the LP-PUL pulsation code is coupled to the LPCODE evolutionary code and is based on a general Newton-Raphson technique that solves the fourth-order (second-order) set of real equations and boundary conditions governing linear, adiabatic, nonradial (radial) stellar pulsations following the dimensionless formulation of Dziembowski (1971; see also, Unno et al. 1989). On the other hand, the nonradial (radial) nonadiabatic version of the LP-PUL pulsation code solves the sixth-order (fourth-order) complex system of linearized equations and boundary conditions as given by Unno et al. (1989; see also Saio et al. 1983). Our nonadiabatic computations rely on the frozen-convection approximation, in which the perturbation of the convective flux is neglected. To compute the Brunt-Väisälä frequency (N), we follow the so-called Ledoux modified treatment (Tassoul et al. 1990; Brassard et al. 1991).

Realistic configurations of the evolutionary sequences for low-mass He-core WD stars were derived by Althaus et al. (2013) by mimicking the binary evolution of progenitor stars. Binary evolution was assumed to be fully nonconservative, and the losses of angular momentum due to mass loss, gravitational wave radiation, and magnetic braking were considered. All of the He-core WD initial models were derived from evolutionary calculations for binary systems consisting of an evolving main-sequence low-mass component (donor star) of initially 1 $M_\odot$ and a 1.4 $M_\odot$ neutron star companion as the other component. A total of 14 initial He-core WD models with stellar masses of 0.1554, 0.1612, 0.1650, 0.1706, 0.1762, 0.1805, 0.1863, 0.1917, 0.2019, 0.2389, 0.2707, 0.3205, 0.3624, and 0.4352 $M_\odot$ were computed for initial orbital periods at the beginning of the Roche lobe phase in the range of 0.9 to 300 d. The evolution of these models was computed down to the range of luminosities of cool WDs,

including the stages of multiple thermonuclear CNO flashes at the beginning of the cooling branch.

3. Asteroseismological analysis

Asteroseismology has so far been applied to infer the fundamental parameters of numerous pulsating WD stars. Specifically, by comparing the observed frequencies (or periods) of pulsating WDs and appropriate theoretical models, it has been possible to infer details about their origin, internal structure, and evolution. The larger the number of frequencies detected in a given pulsating WD, the more information can be inferred, such as gravity, effective temperature, stellar mass, and also the internal chemical stratification, the rate of rotation, the existence of magnetic fields, the cooling timescale, and the core composition, to name a few. For instance, the works of Bradley (1998), Romero et al. (2012) and Giammichele et al. (2016, 2017a,b) have proven that asteroseismology is a powerful technique for exploring the interior of WDs.

In the next subsections, we describe the asteroseismological methods we employed.

3.1. Searching for a constant period spacing

In the asymptotic limit of high-radial order k, nonradial g modes with the same harmonic degree ℓ are expected to be equally spaced in period (Tassoul 1980):

$$\Delta\Pi_\ell^a = \Pi_{k+1,\ell} - \Pi_{k,\ell} = \frac{2\pi^2}{\sqrt{\ell(\ell+1)}}\left[\int_0^{R_\star}\frac{N(r)}{r}dr\right]^{-1}, \qquad (1)$$

where N is the Brunt-Väisälä frequency. In principle, the asymptotic period spacing or the average of the computed period spacings calculated from a grid of models (with different masses and effective temperatures) can be compared with the mean period spacing exhibited by a pulsating WD star, and then a value of the stellar mass can be inferred. The initial step to do so is to obtain (if it exists) a mean period spacing underlying the observed periodicities. We searched for a constant period spacing in the data of the target stars by using the Kolmogorov-Smirnov (K-S; see Kawaler 1988), the inverse variance (I-V; see O'Donoghue 1994) and the Fourier transform (F-T; see Handler et al. 1997) significance tests. In the K-S test, the quantity Q is defined as the probability that the observed periods are randomly distributed. Thus, any uniform – or at least systematically nonrandom – period spacing present in the period spectrum of the star under analysis will appear as a minimum in Q. In the I-V test, a maximum of the inverse variance will indicate a constant period spacing. Finally, in the F-T test, we calculate the Fourier transform of a Dirac comb function (created from a set of observed periods), and then we plot the square of the amplitude of the resulting function in terms of the inverse of the frequency. Once again, a maximum in the square of the amplitude will indicate a constant period spacing.

Tables 2 to 10 show that the number of periods exhibited by all the known ELMV WDs varies from 2 to 7. In particular, because of the few periods exhibited by J1614, J2228, J1738, J1618 and J2139, it is not possible to search for a constant period spacing in these cases. For J1840, J1112, J1518 and J1735, however, we were able to carry out this procedure. Unfortunately, for J1840 and J1112, we were unable to estimate any unambiguous constant period spacing, and furthermore, there was no agreement between the significance tests. The reason might be that
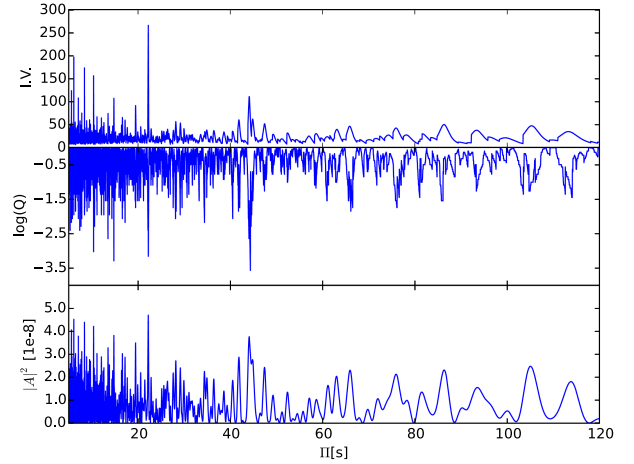

Fig. 2. I-V (*upper panel*), K-S (*middle panel*), and F-T significance (*bottom panel*) tests applied to the period spectrum of J1518 to search for a constant period spacing. The periods used here are those indicated in Table 4.
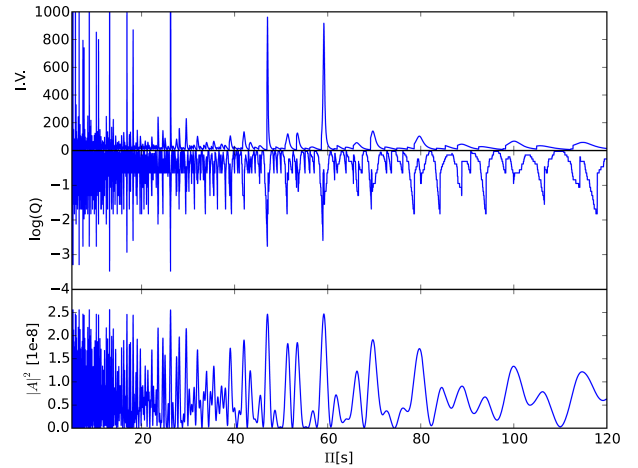

Fig. 3. Same as Fig. 2, but for J1735. The periods used here are those indicated in Table 9.

the periods exhibited by these stars are not fully in the asymptotic regime and/or there are not as many periods as required to determine a mean period spacing. However, for J1518 and J1735, as shown in Figs. 2 and 3, respectively, we found clear indication of a constant period spacing for the three independent significance tests for both stars. For J1518, it lies at roughly $\Delta\Pi \sim 44$ s, although there is also another possible value at ~ 22.2 s, both for the three significance tests. However, the latter is too short and probably represents the harmonic of the main period spacing ($\frac{1}{2}\Delta\Pi$). In addition, a period separation of ~ 22 s is not likely to be the asymptotic period spacing because the resulting stellar mass would be prohibitively high (Córsico & Althaus 2014a). We therefore assume that the period spacing associated with J1518 is $\Delta\Pi^O \sim 44$ s. In the case of J1735, there is a possible value for the period spacing at ~ 26 s, but once again, as we mentioned before, this value is too low and we discarded it. Two other possibilities are at ~ 47 s and ~ 59 s, the latter being a more expectable value for the period spacing, according to the asymptotic predictions. We therefore adopt $\Delta\Pi^O \sim 59$ s as the period spacing for this star.
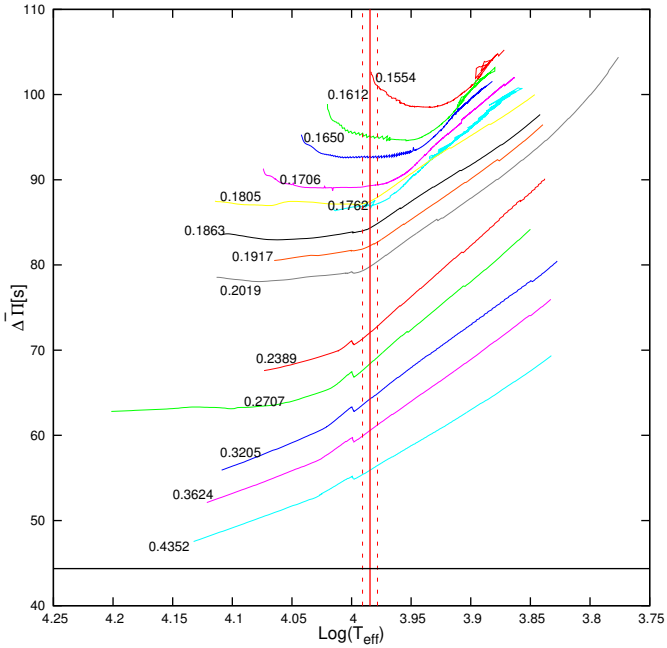
Fig. 4. Average of the computed dipole ($\ell = 1$) period spacings ($\overline{\Delta\Pi_\ell}$) assessed in the range of the periods observed in J1518, corresponding to each WD model sequence considered in this work, in terms of the logarithm of the effective temperature. Numbers along each curve denote the stellar mass (in solar units). The observed period spacing derived for J1518 is depicted with a horizontal solid line. We also indicate the $T_{\rm eff}$ (vertical solid line) in the 3D model, together with its uncertainties (vertical dashed lines).

3.2. Determination of the stellar mass of J1518 and J1735 from the observed period spacing

In this section, we aim to estimate the masses of J1518 and J1735 by comparing the average of the computed period spacings ($\overline{\Delta\Pi_\ell}$) for our grid of models with the observed period spacing ($\Delta\Pi_\ell^{\rm O}$) determined in the previous section for each star. We caution that this approach is problematic: the period spacing in this type of stars could also be sensitive to the thickness of the outer H envelope in addition to the stellar mass (Tassoul et al. 1990; Fontaine & Brassard 2008). We defer a full exploration of this dependence to a future publication.

The average of the computed period spacings is assessed as $\overline{\Delta\Pi_\ell} = (n-1)^{-1} \sum_k \Delta\Pi_k$, where the "forward" period spacing is defined as $\Delta\Pi_k = \Pi_{k+1} - \Pi_k$ (k being the radial order), and n is the number of theoretical periods within the range of the periods observed in the target star. For J1518, $\Pi_k \in [1330, 3900]$ s, while for J1735, $\Pi_k \in [3350, 5000]$ s.

In Fig. 4 we show the run of the average of the computed period spacings ($\ell = 1$) for J1518 in terms of the logarithm of the effective temperature for our ELM WD evolutionary sequences, along with the observed period spacing for J1518. The figure shows that the lower the values of $\overline{\Delta\Pi_\ell}$, the greater the stellar mass. In this case, it clearly shows that such a low value (~44 s) of the observed period spacing would lead to a stellar mass greater than $0.4352\,M_\odot$, which is higher than expected for this type of stars. Hence, this analysis does not seem to lead to a proper value of the mass for J1518. The reason might be that this star is not pulsating in the asymptotic regime (see Córsico & Althaus 2014a).

In Fig. 5 we show the run of the average of the computed period spacings ($\ell = 1$) for J1735 in terms of the logarithm of the
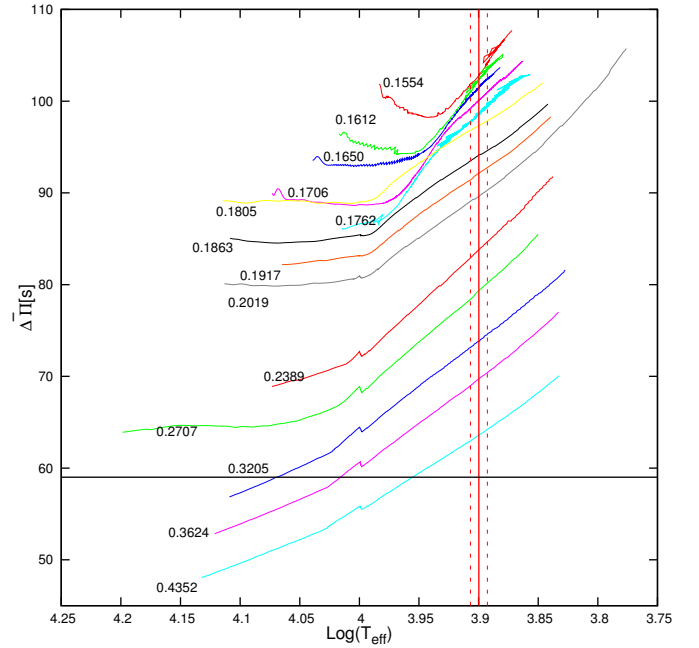
Fig. 5. Same as Fig. 4, but for J1735.

effective temperature for our ELM WD evolutionary sequences, along with the observed period spacing for J1735. Once again, the value we obtain for the stellar mass is higher than expected ($\gtrsim 0.43\,M_\odot$), even though this star may be pulsating in the asymptotic regime. Alternatively, if the value we have obtained for the observed period spacing is real, in the sense that it can be associated with the behavior of high radial order g modes, then it would indicate that this star has a mass somewhat higher than $0.4352\,M_\odot$, and that their spectroscopic parameters ($T_{\rm eff}, \log g$) could be incorrect.

In the next section we follow another approach to estimate the stellar mass and other features of all the known ELMVs through the search of theoretical models that best fit the individual observed periods. The advantage of this procedure is that once we have chosen a model, we have access to information of the star that is otherwise very difficult (if not impossible) to obtain by any other method.

3.3. Constraints from the individual observed periods: searching for the best-fit model

In this approach we search for a pulsation model that best matches the individual pulsation periods of a given star under study. The goodness of the match between the theoretical pulsation periods ($\Pi_k^{\rm T}$) and the observed individual periods ($\Pi_i^{\rm O}$) is measured by means of a merit function defined as

$$\chi^2(M_\star, T_{\rm eff}) = \frac{1}{m} \sum_{i=1}^{m} \min\left[\left(\Pi_i^{\rm O} - \Pi_k^{\rm T}\right)^2\right], \qquad (2)$$

where m is the number of observed periods. The ELM model that shows the lowest value of χ^2, if exists, is adopted as the best-fit model. We assess the function $\chi^2 = \chi^2(M_\star, T_{\rm eff})$ for stellar masses of 0.1554, 0.1612, 0.1650, 0.1706, 0.1762, 0.1805, 0.1863, 0.1917, 0.2019, 0.2389, 0.2707, 0.3205, 0.3624, and $0.4352\,M_\odot$. For the effective temperature we also cover a wide range: $13\,000 \gtrsim T_{\rm eff} \gtrsim 6000$ K.

We have carried out asteroseismological fits for all the known ELMV WD stars. This is the first time that this procedure
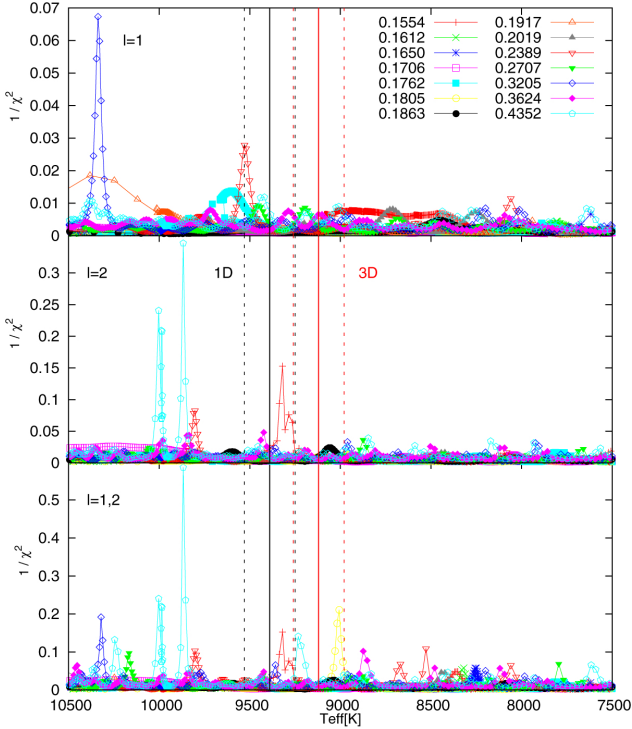
Fig. 6. Inverse of the quality function of the period fit considering $\ell = 1$ (*top panel*), $\ell = 2$ (*middle panel*), and $\ell = 1, 2$ (*bottom panel*) versus T_{eff} for J1840 (see text for details). The vertical strips depict the spectroscopic T_{eff} (solid vertical lines) and their uncertainties (dashed vertical lines) for the 1D (dark gray lines) and 3D models (red lines).

Fig. 7. Same as Fig. 6, but for J1112 for the five longest periods.

is used for this type of stars. We started our analysis assuming that all of the observed periods correspond to g modes associated with $\ell = 1$, and considering the set of observed periods, Π_i^O, of each star to compute the quality function given by Eq. (2). Next, we considered the case in which all of the observed periods correspond to g modes associated with $\ell = 2$, and finally, we considered the case of a mix of g modes associated with $\ell = 1$ and $\ell = 2$. In the case of J1112, we performed a more detailed analysis. For this star we worked with two different sets of observed periods. On the one hand, the five longest periods, for which we carried out the analysis previously mentioned. On the other hand, we adopted the whole set of periods (seven) and explored the possibility that they correspond to a mix of g and p modes with $\ell = 1$, and we also considered the case in which the observed periods correspond to radial ($\ell = 0$) and p and g modes ($\ell = 1, 2$).

Figures 6 to 15 show the quantity $(\chi^2)^{-1}$ in terms of the effective temperature for different stellar masses for each known ELMV, taking the corresponding set of observed periods into account. We also include the effective temperatures and their uncertainties for the 1D (dark gray vertical lines) and 3D model atmosphere (red vertical lines) determinations. As mentioned before, the goodness of the match between the theoretical and the observed periods is measured by the value of χ^2: the better the period match, the lower the value of χ^2 – in the figures, the greater the value of $(\chi^2)^{-1}$. In some cases, there is a single maximum, and we adopt that model as the asteroseismological solution for that star. Sometimes, there are multiple possible solutions, and we need to employ some external constraint in order to choose one. Generally, the constraint is the uncertainty in the effective temperature, given by the spectroscopy. In some cases, when there are still multiple possible solutions, we choose
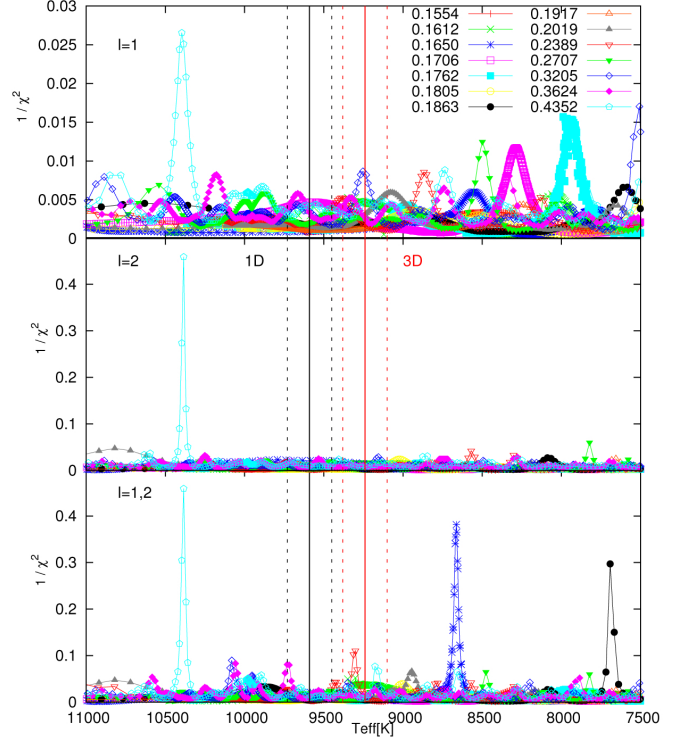
a model with a mass as close as possible to the mass given by the spectroscopic determinations. It is important to mention that as it is more likely to observe $\ell = 1$ than $\ell = 2$ modes (because geometric cancellation effects become stronger with higher values of ℓ; see Dziembowski 1977), we typically chose, when possible, the asteroseismological solutions that fit observed periods with a larger number of $\ell = 1$ modes.

3.3.1. The case of J1840

In Fig. 6 we show the match between the theoretical and the five observed periods of J1840, assuming they are associated with g modes, for the cases of $\ell = 1$ (top panel), $\ell = 2$ (middle panel), and $\ell = 1, 2$ (bottom panel). The case $\ell = 2$ is only depicted for the sake of completeness, since we do not expect that a pulsating star can exhibit all the periods associated with $\ell = 2$ and none of them correspond to $\ell = 1$ because of geometric cancellation arguments (see above). For the $\ell = 1$ case, the upper panel shows that there is more than one solution. In particular, the absolute maximum (the best solution) lies at a much higher effective temperature than that allowed by both spectroscopic determinations. The second-best solution lies within the range of allowed T_{eff} for the 1D model atmosphere ($T_{eff} = 9390 \pm 140$ K), so that we may adopt this model because it represents a good period fit. It corresponds to a mass of $M_\star = 0.2389\ M_\odot$ at $T_{eff} \sim 9529$ K. For the $\ell = 1, 2$ case, once again there is no a single solution, and the best period fit has a very high value of T_{eff}. In the ranges of allowed T_{eff}, there is no unambiguous asteroseismological model. However, we may adopt the solution given for the model with $M_\star = 0.1805\ M_\odot$ at $T_{eff} \sim 9007$ K, which is the best fit in the range of allowed T_{eff} for the 3D model atmosphere ($T_{eff} = 9120 \pm 140$ K).

In order to determine how good the agreement of theoretical and observed periods is, we can compare them by computing the absolute period differences $|\delta\Pi| = |\Pi^O - \Pi^T|$. The results for
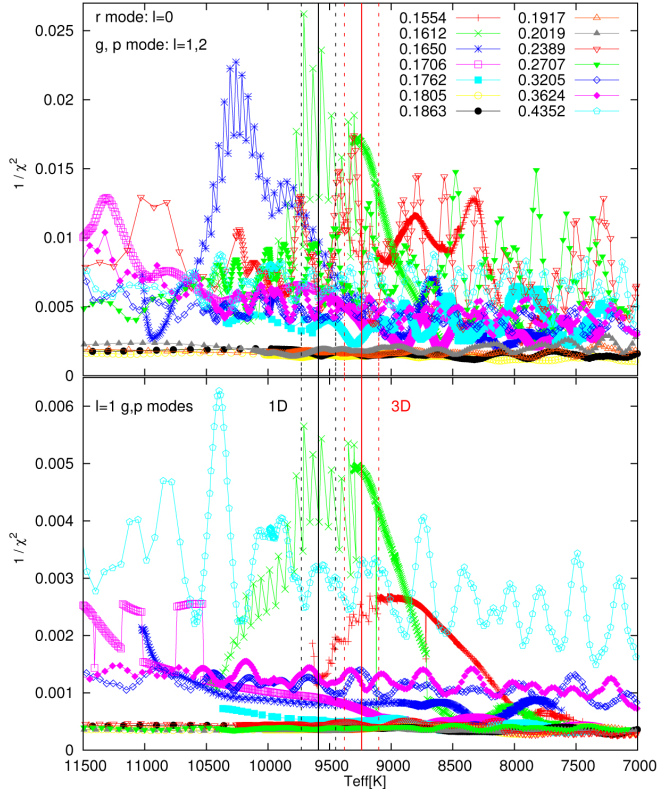
Fig. 8. Same as Fig. 7, but for the case of the seven observed periods of J1112. In *the upper panel*, the case of radial ($\ell = 0$) and p and g modes ($\ell = 1, 2$) is shown, while in *the bottom panel* the case of p and g modes with $\ell = 1$ is displayed.

Table 11. Comparison of the observed and theoretical periods for J1840, corresponding to the asteroseismological model with $M_\star = 0.2389\ M_\odot$ and $T_{\rm eff} = 9529$ K ($\ell = 1$).

$\Pi^{\rm O}[s]$	$\Pi^{\rm T}[s]$	ℓ	k	$|\delta\Pi|[s]$	$\eta[10^{-5}]$	Remark
1164.15	1168.26	1	14	4.11	0.0345	unstable
1578.70	1589.47	1	20	10.77	0.384	unstable
2376.07	2378.49	1	31	2.42	2.61	unstable
3930.0	3923.65	1	52	6.35	4.72	unstable
4445.3	4445.20	1	59	0.1	4.16	unstable

Notes. We also show the harmonic degree ℓ, the radial order k, the absolute period difference, and the nonadiabatic growth rate for each theoretical period.

J1840 are shown in Table 11 for the case of $\ell = 1$. Column 6 of Table 11 shows the value of the linear nonadiabatic growth rate (η), defined as $\eta\ (\equiv -\Im(\sigma)/\Re(\sigma)$, where $\Re(\sigma)$ and $\Im(\sigma)$ are the real and the imaginary part, respectively, of the complex eigenfrequency σ, computed with the nonadiabatic version of the LP-PUL pulsation code (Córsico et al. 2006; Córsico & Althaus 2016). A value of $\eta > 0$ ($\eta < 0$) implies an unstable (stable) mode (see column 6 of Table 11). For $\ell = 1, 2$ the results are shown in Table 12.

Considering that the period fit of the $\ell = 1, 2$ case is better because it has a higher value of $(\chi^2)^{-1}$ than the solution of the $\ell = 1$ case, and the mass of this model ($M_\star = 0.1805\ M_\odot$) is in line with the spectroscopic masses determined for this star ($M_\star^{\rm (1D)} = 0.183\ M_\odot$ and $M_\star^{\rm (3D)} = 0.177\ M_\odot$), we adopt the model with $M_\star = 0.1805\ M_\odot$ and $T_{\rm eff} = 9007$ K as the asteroseismological
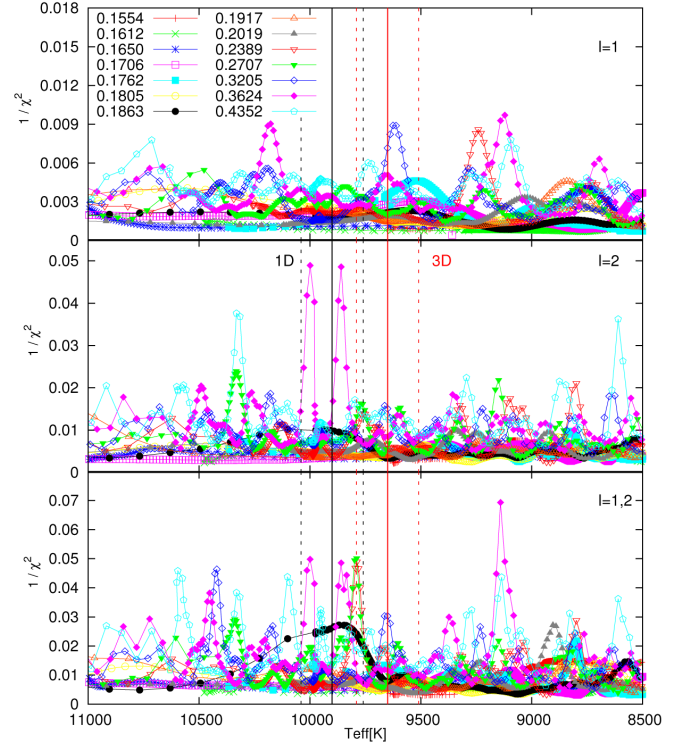
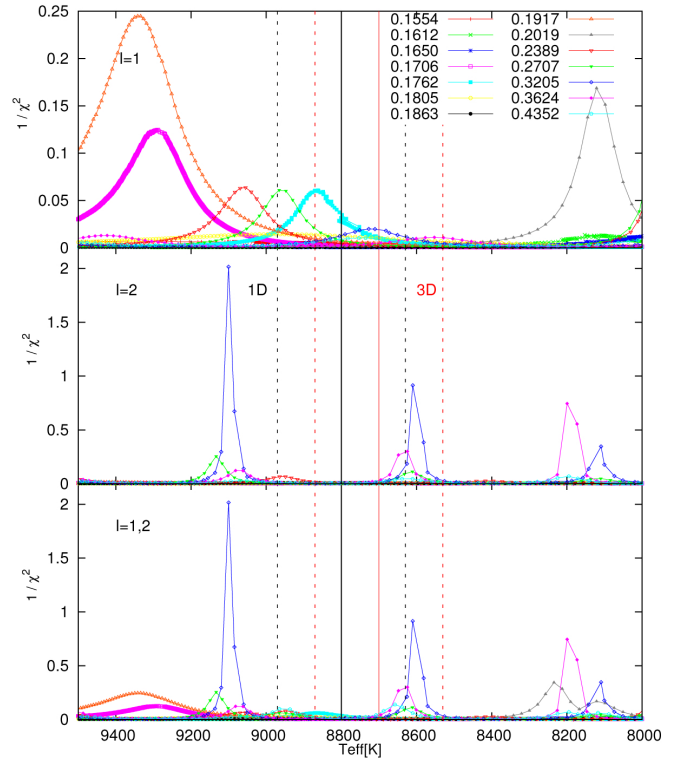**Fig. 9.** Same as Fig. 6, but for the case of J1518.

Fig. 10. Same as Fig. 6, but for J1614.

solution for J1840, which has a value of $T_{\rm eff}$ in agreement with the spectroscopy (for the 3D model), even though this model has more $\ell = 2$ than $\ell = 1$ modes. We note that most of the periods of this model correspond to pulsationally unstable modes.
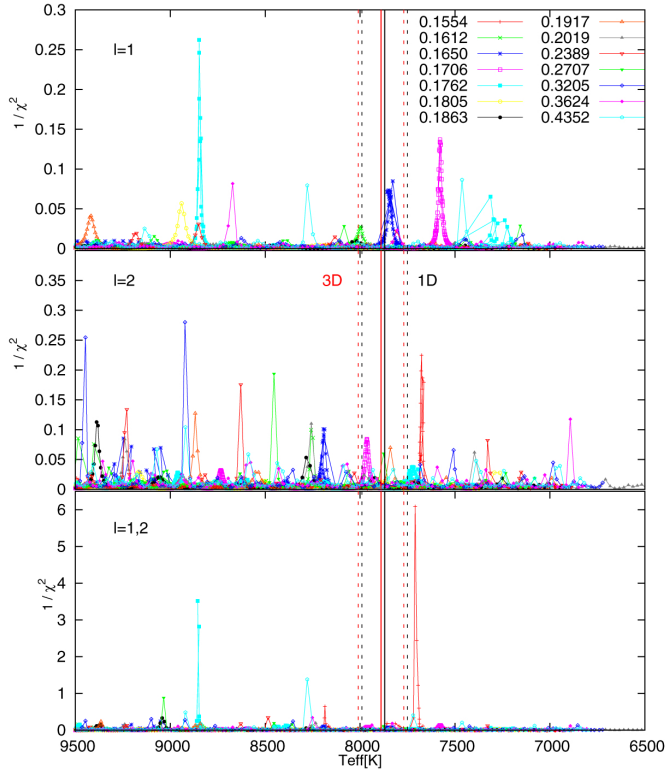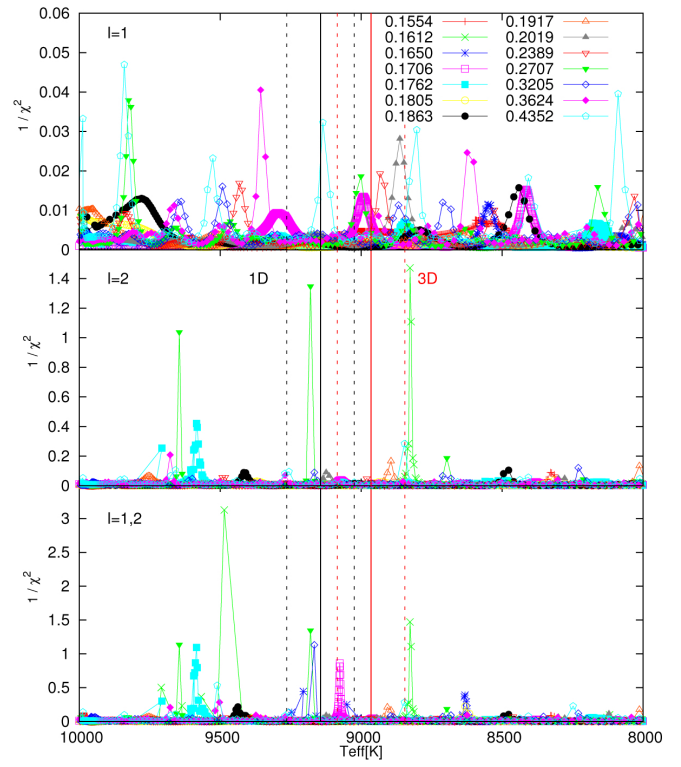
Fig. 11. Same as Fig. 6, but for J2228.

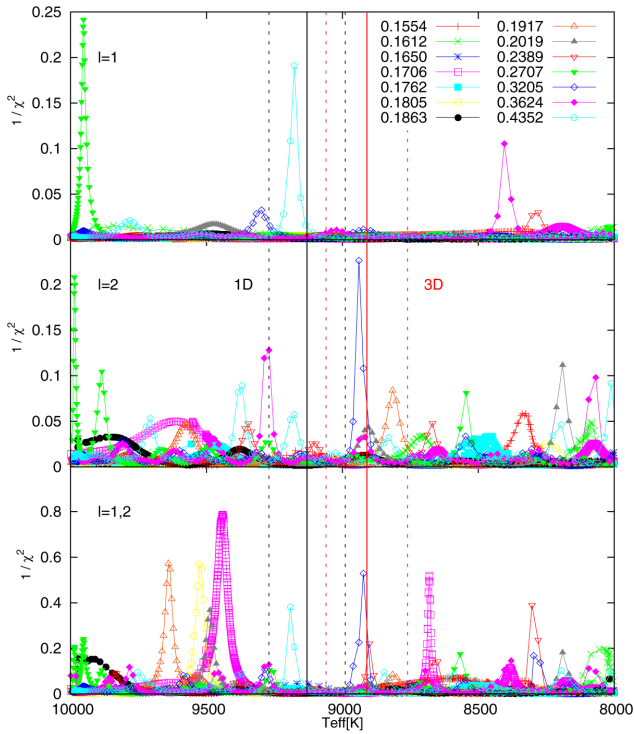**Fig. 13.** Same as Fig. 6, but for J1618.

Fig. 12. Same as Fig. 6, but for J1738.
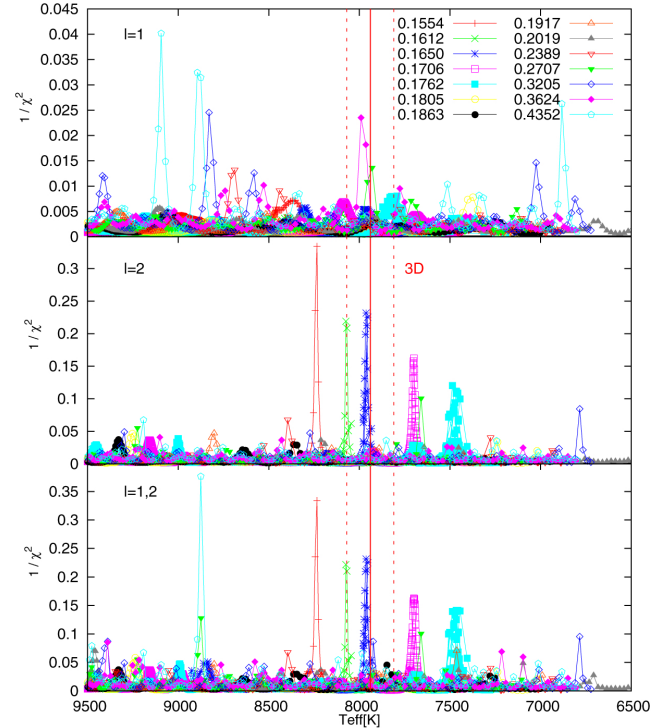
Fig. 14. Same as Fig. 6, but for J1735.

3.3.2. The case of J1112

Because of the two short periods at $\sim$108 s and $\sim$134 s in the pulsation spectrum of J1112, which are probably associated with p or radial modes, we divided the analysis for this star into two parts: on the one hand, we considered the five longest observed periods, assuming that they are all associated with $\ell = 1$, $\ell = 2$ g modes or a mix of $\ell = 1$ and $\ell = 2$ g modes. On the other hand, we considered the whole set of periods (seven), considering first, that they are associated with a mix of $\ell = 1$ p and g modes[1], and second, with a mix of p and g modes with $\ell = 1$ and $\ell = 2$,

---

[1] We have also explored a possible combination of g and p modes with $\ell = 1$ and $\ell = 2$, but we did not obtain significantly different results.

Fig. 15. Same as Fig. 6, but for J2139.

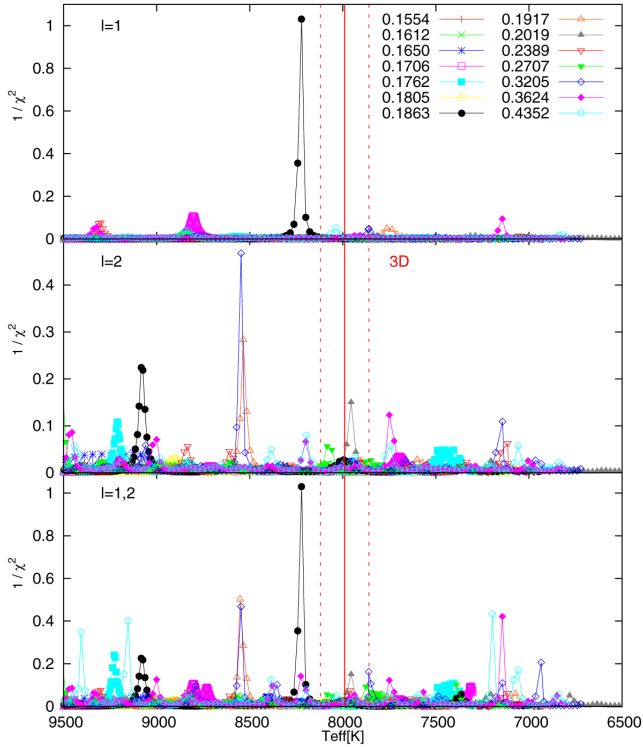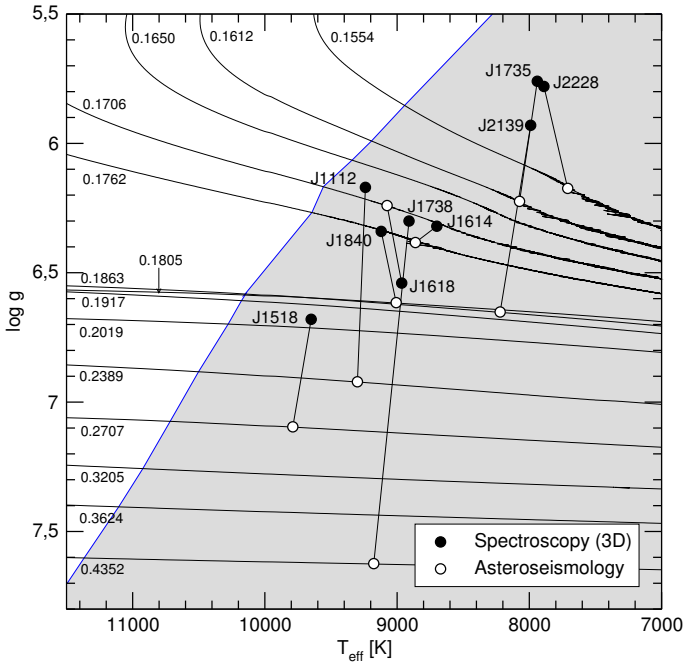**Fig. 16.** Location of the nine analyzed stars, according to the spectroscopic parameters from the 3D model-atmosphere (black circles), and the corresponding asteroseismological models adopted for each star (white circles), along with our evolutionary tracks of low-mass He-core WDs in the $\log T_{\rm eff} - \log g$ plane. The gray-shaded region bounded by the thin blue line corresponds to the instability domain of $\ell = 1$ g modes according to the nonadiabatic computations of Córsico & Althaus (2016).

and also radial modes ($\ell = 0$). At this point, it is worth mentioning that the reality of these two short periods are not definitively confirmed, as claimed by Hermes et al. (2013b). It is therefore worthwhile performing these separate analyses.

Table 12. Same as Table 11, but for the model with $M_\star = 0.1805\ M_\odot$ and $T_{\rm eff} = 9007$ K, in the case of $\ell = 1, 2$, adopted for J1840.

$\Pi^{\rm O}$[s]	$\Pi^{\rm T}$[s]	ℓ	k	$|\delta\Pi|$[s]	$\eta[10^{-6}]$	Remark
1164.15	1163.53	2	20	0.62	0.719	unstable
1578.70	1577.75	2	28	0.95	2.47	unstable
2376.07	2373.77	2	43	2.30	4.13	unstable
3930.0	3933.98	2	72	3.98	-3.22	stable
4445.3	4444.16	1	47	1.14	6.96	unstable

Table 13. Same as Table 11, but for J1112 (for the five longest periods) for the model with $M_\star = 0.3205\ M_\odot$ and $T_{\rm eff} = 9253$ K, in the case of $\ell = 1$.

$\Pi^{\rm O}$[s]	$\Pi^{\rm T}$[s]	ℓ	k	$|\delta\Pi|$[s]	$\eta[10^{-6}]$	Remark
1792.905	1802.269	1	26	9.364	4.90	unstable
1884.599	1867.419	1	27	17.18	4.87	unstable
2258.528	2264.984	1	33	6.456	5.54	unstable
2539.695	2530.317	1	37	9.378	5.91	unstable
2855.728	2863.702	1	42	7.974	5.08	unstable

Table 14. Same as Table 13 for J1112 (in the case of the five longest periods), but for the model with $M_\star = 0.2389\ M_\odot$ and $T_{\rm eff} = 9300$ K, in the case of $\ell = 1, 2$.

$\Pi^{\rm O}$[s]	$\Pi^{\rm T}$[s]	ℓ	k	$|\delta\Pi|$[s]	$\eta[10^{-6}]$	Remark
1792.905	1798.677	2	40	5.772	6.71	unstable
1884.599	1884.824	2	42	0.225	6.63	unstable
2258.528	2259.902	1	29	1.374	7.13	unstable
2539.695	2536.648	2	57	3.047	3.79	unstable
2855.728	2856.498	1	37	0.77	11.2	unstable

In Fig. 7 we show the match between the theoretical and the five longest observed periods of J1112, assuming they are associated with g modes, for the cases of $\ell = 1$ (top panel), $\ell = 2$ (middle panel, shown for completeness), and $\ell = 1, 2$ (bottom panel). In the case of $\ell = 1$, the absolute maximum is at a very high effective temperature, and there are also many other solutions for low values of $T_{\rm eff}$. Within the range of allowed $T_{\rm eff}$ for the 3D model atmosphere analysis ($T_{\rm eff} = 9240 \pm 140$ K), there may be a solution for the model with $M_\star = 0.3205\ M_\odot$ at $T_{\rm eff} \sim 9253$ K. We compare the observed and the theoretical periods as we did for the previous star, and the results are displayed in Table 13. If we consider the case of $\ell = 1, 2$, there are multiple local maxima that are either too hot or too cold in comparison with the allowed values of $T_{\rm eff}$. Nevertheless, there may be a possible solution within the range of allowed $T_{\rm eff}$ (for the 3D model) for the case of $M_\star = 0.2389\ M_\odot$ at $T_{\rm eff} \sim 9300$ K. In Table 14 we show the comparison between the observed and the theoretical periods for this model.

Next, we considered the case in which the whole set of observed periods (seven) corresponds to p and g modes with $\ell = 1$, and also the case in which it corresponds to radial ($\ell = 0$) and p and g modes ($\ell = 1, 2$). The results are shown in Fig. 8. For the case of the mix of p and g modes with $\ell = 1$ (bottom panel), the absolute maximum lies at a high value of $T_{\rm eff}$ and there is no unambiguous solution in the allowed ranges of $T_{\rm eff}$. However, there may be one possible solution for $M_\star = 0.1612\ M_\odot$ that lies in the allowed range of $T_{\rm eff}$ for the 1D model ($T_{\rm eff} = 9590 \pm 140$ K). In a more complete analysis, considering the mix of radial ($\ell = 0$) and p and g modes ($\ell = 1, 2$), we find that the absolute maximum

Table 15. Same as Table 13 for J1112 (considering the whole set of periods), but for the model with $M_\star = 0.1612\ M_\odot$ and $T_{\text{eff}} = 9709$ K, in the case of p, g ($\ell = 1, 2$), and radial modes ($\ell = 0$).

Π^O[s]	Π^T[s]			ℓ	k	$|\delta\Pi|$[s]	$\eta[10^{-7}]$	Remark
	g	p	Radial					
107.56	–	–	105.176	0	1	2.384	−0.287	stable
134.275	–	136.881	–	2	0	2.606	−0.0238	stable
1792.905	1793.216	–	–	1	17	0.311	−0.0197	stable
1884.599	1889.869	–	–	2	32	5.270	−7.34	stable
2258.528	2272.008	–	–	2	39	13.480	−53.6	stable
2539.695	2543.853	–	–	2	44	4.158	−196	stable
2855.728	2850.465	–	–	1	28	5.263	−2.52	stable

is at the same model and it represents a better match because it has a higher value of $(\chi^2)^{-1}$, as shown in the top panel of Fig. 8. It is the best period fit for this case, and corresponds to $M_\star = 0.1612\ M_\odot$ at $T_{\text{eff}} \sim 9709$ K. Hence, this represents a very good solution for the case of the whole set of periods. Once again, we show the comparison between the observed and the theoretical periods in Table 15. This table shows that one of the short periods may be associated with a p mode (with $\ell = 2$) and the other period a radial mode ($\ell = 0$).

Considering all the results from this analysis, we may conclude that the best solution corresponds to the model with $M_\star = 0.1612\ M_\odot$ and $T_{\text{eff}} = 9709$ K, which is quite in line with the spectroscopic masses determined for this star ($M_\star^{(1D)} = 0.179\ M_\odot$ and $M_\star^{(3D)} = 0.169\ M_\odot$) and also in line with the T_{eff} given by the spectroscopy (for the 1D model). Unfortunately, our nonadiabatic computations (see Table 15) predict that all the modes of this possible solution are pulsationally stable, which forces us to discard this solution. When we consider this and ignore the two shortest periods of this star, we could adopt the solution that is found with a mass of $M_\star = 0.2389\ M_\odot$ and $T_{\text{eff}} = 9300$ K (see Table 14), although this value of the stellar mass does not agree as well with the masses resulting from the spectroscopy. We note, however, that all the periods of this model are associated with pulsationally unstable modes. Finally, the fact that we are not able to find an asteroseismological model with unstable modes with periods that fit the seven periods observed in J1112 (including the shortest ones) could be indicating that the periods at ∼108 s and ∼134 s reported by Hermes et al. (2013b) are not real. This calls for the need of further photometric work on this star.

3.3.3. The case of J1518

In Fig. 9 we show the match between the theoretical periods and the seven observed periods of J1518 assuming they are associated with g modes for the cases of $\ell = 1$ (top panel), $\ell = 2$ (middle panel), and $\ell = 1, 2$ (bottom panel). In the $\ell = 1$ case, we see multiple local maxima. However, in the range of allowed T_{eff} given by the 3D model atmosphere calculations ($T_{\text{eff}} = 9650 \pm 140$ K), there is a possible solution that may be chosen as a representative model for J1518. This corresponds to $M_\star = 0.3205\ M_\odot$ at $T_{\text{eff}} \sim 9625$ K. In Table 16 we compare the theoretical and the observed periods for this model. For the case of $\ell = 1, 2$, the best period fit lies at a very low T_{eff}, and there are multiple local maxima within the ranges of allowed T_{eff}. However, there is a possible solution characterized by $M_\star = 0.2707\ M_\odot$ and $T_{\text{eff}} \sim 9789$ K, which, although not so clear in the figure, is the best period fit that lies within the ranges of allowed T_{eff} ($T_{\text{eff}}^{(1D)} = 9900 \pm 140$ K and $T_{\text{eff}}^{(3D)} = 9650 \pm 140$ K).

Table 16. Same as Table 11, but for J1518 for the model with $M_\star = 0.3205\ M_\odot$ and $T_{\text{eff}} = 9625$ K in the case of $\ell = 1$.

Π^O[s]	Π^T[s]	ℓ	k	$|\delta\Pi|$[s]	$\eta[10^{-5}]$	Remark
1335.318	1324.926	1	19	10.392	0.484	unstable
1956.361	1953.996	1	29	2.365	1.71	unstable
2134.027	2146.419	1	32	12.392	2.26	unstable
2268.203	2275.543	1	34	7.340	2.46	unstable
2714.306	2727.475	1	41	13.169	2.49	unstable
2799.087	2791.464	1	42	7.623	2.57	unstable
3848.201	3832.927	1	58	15.274	0.0899	unstable

Table 17. Same as Table 16, but for the model adopted for J1518 with $M_\star = 0.2707\ M_\odot$ and $T_{\text{eff}} = 9789$ K in the case of $\ell = 1, 2$.

Π^O[s]	Π^T[s]	ℓ	k	$|\delta\Pi|$[s]	$\eta[10^{-5}]$	Remark
1335.318	1331.485	2	32	3.833	3.94	unstable
1956.361	1960.394	2	48	4.033	5.37	unstable
2134.027	2140.805	1	30	6.778	5.25	unstable
2268.203	2274.699	1	32	6.496	6.55	unstable
2714.306	2714.827	2	67	0.521	0.711	unstable
2799.087	2794.753	2	69	4.334	−0.357	stable
3848.201	3847.023	1	55	1.178	7.81	unstable

We present in Table 17 the comparison between the observed and the theoretical periods for this case.

Considering that the solution for the $\ell = 1, 2$ case implies a much better fit (a higher value of $(\chi^2)^{-1}$) than the one for the $\ell = 1$ case, we may adopt the model with $M_\star = 0.2707\ M_\odot$ and $T_{\text{eff}} = 9789$ K as the asteroseismological solution for this star, which is in line with the T_{eff} given by the spectroscopy. Moreover, most of the periods of the adopted model are associated with pulsationally unstable modes. It is necessary to stress, however, that none of the solutions found are in good agreement with the masses resulting from the spectroscopic determinations ($M_\star^{(1D)} = 0.220\ M_\odot$ and $M_\star^{(3D)} = 0.197\ M_\odot$).

3.3.4. The case of J1614

In Fig. 10 we depict the match between the theoretical and the two observed periods of J1614, assuming they are associated with g modes, for the cases of $\ell = 1$ (top panel), $\ell = 2$ (middle panel), and $\ell = 1, 2$ (bottom panel). It is worth mentioning in advance that this period fit is not reliable because this star only shows two independent periods.

In the case of $\ell = 1$, there is no unambiguous solution, and the best solutions are located beyond the ranges of allowed T_{eff}.

Table 18. Same as Table 11, but for the model adopted for J1614 with $M_\star = 0.1762\ M_\odot$ and $T_{\rm eff} = 8862$ K in the case of $\ell = 1$.

$\Pi^{\rm O}$[s]	$\Pi^{\rm T}$[s]	ℓ	k	$|\delta\Pi|$[s]	$\eta[10^{-9}]$	Remark
1184.106	1179.527	1	11	4.579	2.03	unstable
1262.668	1266.119	1	12	3.451	2.88	unstable

Table 19. Same as Table 18 for J1614, but for the model with $M_\star = 0.3205\ M_\odot$ and $T_{\rm eff} = 8610$ K in the case of $\ell = 1, 2$.

$\Pi^{\rm O}$[s]	$\Pi^{\rm T}$[s]	ℓ	k	$|\delta\Pi|$[s]	$\eta[10^{-7}]$	Remark
1184.106	1182.674	2	28	1.432	4.41	unstable
1262.668	1263.035	2	30	0.367	4.13	unstable

However, we may choose the model with $M_\star = 0.1762\ M_\odot$ and $T_{\rm eff} \sim 8862$ K that lies within the ranges of allowed $T_{\rm eff}$ ($T_{\rm eff}^{\rm (1D)} = 8800 \pm 170$ K and $T_{\rm eff}^{\rm (3D)} = 8700 \pm 170$ K), and also has a mass value consistent with the spectroscopic determinations. In Table 18 we show the comparison between the observed and the theoretical periods for this model. In the case of $\ell = 1, 2$, the best fit is located at a high value of $T_{\rm eff}$, but the second-best fit lies within the range of allowed $T_{\rm eff}$ (for the 3D model). It is characterized by $M_\star = 0.3205\ M_\odot$, at $T_{\rm eff} \sim 8610$ K. However, as can be seen in Table 19, the comparison between the observed and the theoretical periods shows that both periods are associated with $\ell = 2$, which is not usually the case because, as already stated, it is more likely to observe periods associated with $\ell = 1$ than $\ell = 2$. Hence, the asteroseismological model we adopt corresponds to the case of $\ell = 1$, with $M_\star = 0.1762\ M_\odot$ and $T_{\rm eff} = 8862$ K, with a mass in line with the spectroscopic determinations ($M_\star^{\rm (1D)} = 0.192\ M_\odot$ and $M_\star^{\rm (3D)} = 0.172\ M_\odot$) and a $T_{\rm eff}$ in agreement with the spectroscopy. Finally, as can be seen from Table 18, both periods are associated with pulsationally unstable modes.

3.3.5. The case of J2228

In Fig. 11 we show the match between the theoretical and the three observed periods of J2228, assuming they are associated with g modes, for the cases of $\ell = 1$ (top panel), $\ell = 2$ (middle panel), and $\ell = 1, 2$ (bottom panel). In the case of $\ell = 1$, there are multiple possible solutions and the best-fit solution is located at a high value of $T_{\rm eff}$. Within the ranges of allowed $T_{\rm eff}$ ($T_{\rm eff}^{\rm (1D)} = 7870 \pm 120$ K and $T_{\rm eff}^{\rm (3D)} = 7890 \pm 120$ K), there is a possible solution for the model with $M_\star = 0.1650\ M_\odot$ at $T_{\rm eff} \sim 7828$ K. In Table 20 we show the comparison between the observed and the theoretical periods for this case. In the case of $\ell = 1, 2$, the absolute maximum lies very close to the ranges of allowed $T_{\rm eff}$. It corresponds to the model with $M_\star = 0.1554\ M_\odot$ at $T_{\rm eff} \sim 7710$ K. In Table 21 we display the comparison between the observed and the theoretical periods for this model.

Since the solution for the case of $\ell = 1, 2$ ($M_\star = 0.1554\ M_\odot$ and $T_{\rm eff} = 7710$ K) implies a much better period fit than the solution for the case of $\ell = 1$, since it lies at a value of $T_{\rm eff}$ almost compatible with the values given by spectroscopy, and because its mass is in line with the spectroscopic determinations for the mass ($M_\star^{\rm (1D)} = 0.152\ M_\odot$ and $M_\star^{\rm (3D)} = 0.142\ M_\odot$), we adopt this model as the asteroseismological solution for J2228. According to our nonadiabatic computations (Table 21), most of the periods of the adopted model are associated with pulsationally unstable modes.

Table 20. Same as Table 11, but for J2228 for the model with $M_\star = 0.1650\ M_\odot$ and $T_{\rm eff} = 7828$ K in the case of $\ell = 1$.

$\Pi^{\rm O}$[s]	$\Pi^{\rm T}$[s]	ℓ	k	$|\delta\Pi|$[s]	$\eta[10^{-8}]$	Remark
3254.5	3259.9	1	31	5.4	4.34	unstable
4178.3	4175.8	1	40	2.5	5.03	unstable
6234.9	6235.2	1	60	0.3	−7.02	stable

Table 21. Same as Table 20, but for the model adopted for J2228 with $M_\star = 0.1554\ M_\odot$ and $T_{\rm eff} = 7710$ K in the case of $\ell = 1, 2$.

$\Pi^{\rm O}$[s]	$\Pi^{\rm T}$[s]	ℓ	k	$|\delta\Pi|$[s]	$\eta[10^{-8}]$	Remark
3254.5	3254.2	2	52	0.3	1.61	unstable
4178.3	4177.9	2	67	0.4	−2.67	stable
6234.9	6234.4	1	58	0.5	0.832	unstable

Table 22. Same as Table 11, but for the model adopted for J1738 with $M_\star = 0.4352\ M_\odot$ and $T_{\rm eff} = 9177$ K in the case of $\ell = 1$.

$\Pi^{\rm O}$[s]	$\Pi^{\rm T}$[s]	ℓ	k	$|\delta\Pi|$[s]	$\eta[10^{-6}]$	Remark
1788	1788.9	1	30	0.9	3.41	unstable
2656	2654.4	1	45	1.6	0.232	unstable
3057	3060.5	1	52	3.5	−4.14	stable

Table 23. Same as Table 22 for J1738, but for the model with $M_\star = 0.4352\ M_\odot$ and $T_{\rm eff} = 9192$ K in the case of $\ell = 1, 2$.

$\Pi^{\rm O}$[s]	$\Pi^{\rm T}$[s]	ℓ	k	$|\delta\Pi|$[s]	$\eta[10^{-6}]$	Remark
1788	1786.7	1	30	1.3	4.45	unstable
2656	2653.6	2	78	2.4	−31.0	stable
3057	3056.5	1	52	0.5	−4.13	stable

3.3.6. The case of J1738

In Fig. 12 we depict the match between the theoretical and the three observed periods of J1738, assuming they are associated with g modes, for the cases of $\ell = 1$ (top panel), $\ell = 2$ (middle panel), and $\ell = 1, 2$ (bottom panel). In the case of $\ell = 1$, the best solution lies at a very high value of $T_{\rm eff}$, but the second-best solution lies within the range of allowed $T_{\rm eff}$ (for the 1D atmosphere model determination, $T_{\rm eff} = 9130 \pm 140$ K). This solution is characterized by $M_\star = 0.4352\ M_\odot$ at $T_{\rm eff} \sim 9177$ K, and the comparison between the observed and the theoretical periods is shown in Table 22. In the case of $\ell = 1, 2$, the absolute maximum is located at a higher effective temperature than the allowed by spectroscopy ($T_{\rm eff} = 9130 \pm 140$ K and $T_{\rm eff} = 8910 \pm 150$ K, 1D and 3D models, respectively), and there are many other solutions. However, the models with $M_\star = 0.3205\ M_\odot$ at $T_{\rm eff} \sim 8922$ K and $M_\star = 0.4352\ M_\odot$ at $T_{\rm eff} \sim 9192$ K are relatively good period fits that lie within the ranges of allowed $T_{\rm eff}$. When we analyze the period-to-period fit in detail, we see that the latter (shown in Table 23) may be more realistic because more modes are associated with $\ell = 1$ than $\ell = 2$. The opposite is true with the former, so we may rather choose the solution with $M_\star = 0.4352\ M_\odot$ although is not the best one.

From this analysis, since the values of $(\chi^2)^{-1}$ for the two possible solutions are not significantly different and the value of the mass is the same for both of them, but the solution for the $\ell = 1$ case has more periods associated with pulsationally unstable modes, we conclude that this is the best asteroseismological solution, characterized by $M_\star = 0.4352\ M_\odot$ and

Table 24. Same as Table 11, but for J1618 for the model with $M_\star = 0.2019\ M_\odot$ and $T_{\rm eff} = 8863$ K in the case of $\ell = 1$.

$\Pi^{\rm O}$[s]	$\Pi^{\rm T}$[s]	ℓ	k	$|\delta\Pi|$[s]	$\eta[10^{-6}]$	Remark
2543.0	2546.46	1	29	3.46	1.70	unstable
4935.21	4927.03	1	57	8.18	0.347	unstable
6125.9	6131.16	1	71	5.26	−4.11	stable

Table 25. Same as Table 24, but for the model adopted for J1618 with $M_\star = 0.1706\ M_\odot$ and $T_{\rm eff} = 9076$ K in the case of $\ell = 1, 2$.

$\Pi^{\rm O}$[s]	$\Pi^{\rm T}$[s]	ℓ	k	$|\delta\Pi|$[s]	$\eta[10^{-4}]$	Remark
2543.0	2541.44	1	26	1.56	0.0144	unstable
4935.21	4934.59	2	91	0.62	3.88	unstable
6125.9	6126.71	2	113	0.81	1.32	unstable

Table 26. Same as Table 11, but for J1735 for the model with $M_\star = 0.3624\ M_\odot$ and $T_{\rm eff} = 7991$ K in the case of $\ell = 1$.

$\Pi^{\rm O}$[s]	$\Pi^{\rm T}$[s]	ℓ	k	$|\delta\Pi|$[s]	$\eta[10^{-6}]$	Remark
3362.76	3356.67	1	48	6.09	−0.660	stable
3834.54	3841.23	1	55	6.69	−1.28	stable
4541.88	4535.74	1	65	6.14	−2.73	stable
4961.22	4954.12	1	71	7.10	−3.83	stable

Table 27. Same as Table 26, but for the model adopted for J1735 with $M_\star = 0.1612\ M_\odot$ and $T_{\rm eff} = 8075$ K in the case of $\ell = 1, 2$.

$\Pi^{\rm O}$[s]	$\Pi^{\rm T}$[s]	ℓ	k	$|\delta\Pi|$[s]	$\eta[10^{-8}]$	Remark
3362.76	3359.87	2	56	2.89	5.57	unstable
3834.54	3831.65	2	64	2.89	0.243	unstable
4541.88	4542.92	2	76	1.04	−14.3	stable
4961.22	4960.70	1	48	0.52	13.9	unstable

$T_{\rm eff} = 9177$ K, which is in line with the $T_{\rm eff}$ given by the spectroscopy (for the 1D model atmosphere computations). However, when we compare the mass of this model with the masses from the spectroscopic determinations ($M_\star^{\rm (1D)} = 0.181\ M_\odot$ and $M_\star^{\rm (3D)} = 0.172\ M_\odot$), we see that they do not agree well. In summary, we cannot find any agreement between the asteroseismological and the spectroscopic results for J1738.

3.3.7. The case of J1618

In Fig. 13 we show the match between the theoretical and the three observed periods of J1618, assuming they are associated with g modes, for the cases of $\ell = 1$ (top panel), $\ell = 2$ (middle panel), and $\ell = 1, 2$ (bottom panel). In the case of $\ell = 1$, there is no unambiguous solution. Within the range of allowed $T_{\rm eff}$ for the 1D model ($T_{\rm eff} = 9144 \pm 120$ K), there is a possible solution for the model with $M_\star = 0.4352\ M_\odot$ at $T_{\rm eff} \sim 9136$ K, and in the range of allowed $T_{\rm eff}$ for the 3D model ($T_{\rm eff} = 8965 \pm 120$ K) there is another possible solution for the model characterized by $M_\star = 0.2019\ M_\odot$ at $T_{\rm eff} \sim 8863$ K. The latter may be more suitable as a solution because its mass is in line with the spectroscopic determinations of the stellar mass (and in comparison, the period fit for the other solution is not significantly better). In Table 24 we show the comparison between the observed and the theoretical periods for the model with $M_\star = 0.2019\ M_\odot$. The panel for the case of a mix of modes with $\ell = 1, 2$ shows an absolute maximum for a higher value of $T_{\rm eff}$ than allowed, and does not show any unambiguous solution in the ranges of allowed $T_{\rm eff}$. However, there is a possible solution characterized by $M_\star = 0.1706\ M_\odot$ at $T_{\rm eff} \sim 9076$ K because although it is not the best period fit in the ranges of allowed $T_{\rm eff}$, it corresponds to modes associated both with $\ell = 1$ and $\ell = 2$ (and not only $\ell = 2$, see Table 25), and the mass is also quite well in line with the mass of the spectroscopic determination.

Although the solution for the $\ell = 1$ case ($M_\star = 0.2019\ M_\odot$) has a mass slightly closer to the masses from the spectroscopic determinations for J1618 ($M_\star^{\rm (1D)} = 0.220\ M_\odot$ and $M_\star^{\rm (3D)} = 0.179\ M_\odot$) than the solution for the $\ell = 1, 2$ case ($M_\star = 0.1706\ M_\odot$), we conclude that the model with $M_\star = 0.1706\ M_\odot$ and $T_{\rm eff} = 9076$ K, is a more suitable solution when we consider that the latter is a better match between the observed and the theoretical periods and also that this value of the stellar mass is more realistic for this type of stars. Moroever, the $T_{\rm eff}$ is in line with the spectroscopy. Hence, this is the model we adopt for

J1618. We note that all of the periods of the adopted model are associated with pulsationally unstable modes.

3.3.8. The case of J1735

In Fig. 14 we plot the match between the theoretical and the four observed periods of J1735 assuming they are associated with g modes, for the cases of $\ell = 1$ (top panel), $\ell = 2$ (middle panel), and $\ell = 1, 2$ (bottom panel). In the $\ell = 1$ case, there are multiple local maxima that have values of $T_{\rm eff}$ that are either too high or too low in comparison with the range of allowed $T_{\rm eff}$ ($T_{\rm eff} = 7940 \pm 130$ K). However, there is a possible solution within that range, corresponding to the model with $M_\star = 0.3624\ M_\odot$ at $T_{\rm eff} \sim 7991$ K. In Table 26 we show the comparison between the observed and the theoretical periods for the mentioned model. We note, however, that in this stellar model, which constitutes a possible seismological solution for J1735, all the modes are pulsationally stable. As for the case of $\ell = 1, 2$, the best-fit models have values of $T_{\rm eff}$ higher than allowed. Although there is a possible solution within the range of allowed $T_{\rm eff}$ for the model characterized by $M_\star = 0.1650\ M_\odot$ at $T_{\rm eff} \sim 7963$ K, when we compare the observed and the theoretical periods, we find that they are all associated with $\ell = 2$. The model with $M_\star = 0.1612\ M_\odot$ that lies at a slightly higher value of $T_{\rm eff}$ than allowed (~ 8075 K) may therefore be a good solution for this case (see Table 27).

Taking into consideration the spectroscopic determination for the mass of J1735, $M_\star^{\rm (3D)} = 0.142 \pm 0.010\ M_\odot$, and comparing the quality of the period fit of the asteroseismological results, we find that the model with $M_\star = 0.1612\ M_\odot$ and $T_{\rm eff} = 8075$ K is an appropriate solution (with the $T_{\rm eff}$ almost compatible with the spectroscopy), and this is the one we adopt. This model has most of its periods associated with pulsationally unstable modes.

3.3.9. The case of J2139

In Fig. 15 we depict the match between the theoretical and the three observed periods of J2139 assuming they are associated with g modes, for the cases of $\ell = 1$ (top panel), $\ell = 2$ (middle panel), and $\ell = 1, 2$ (bottom panel). In the first case, the absolute maximum, located at $T_{\rm eff} \sim 8221$ K for a model with $M_\star = 0.1863\ M_\odot$, is very close to the range of allowed $T_{\rm eff}$ ($T_{\rm eff} = 7990 \pm 130$ K). Then, it represents a good solution. In

Table 28. Same as Table 11, but for the model adopted for J2139 with $M_\star = 0.1863\, M_\odot$ and $T_{\rm eff} = 8221$ K in the case of $\ell = 1$.

$\Pi^{\rm O}[s]$	$\Pi^{\rm T}[s]$	ℓ	k	$|\delta\Pi|[s]$	$\eta[10^{-7}]$	Remark
2119.44	2120.01	1	22	0.57	1.14	unstable
2482.32	2483.89	1	26	1.57	1.74	unstable
3303.3	3303.63	1	35	0.33	2.19	unstable

the case of a mix of modes with $\ell = 1, 2$, the absolute maximum corresponds to the same model, and the three periods are associated with $\ell = 1$. There are other possible solutions, but they lie far from the range of allowed $T_{\rm eff}$, and inside this range, the fits are poor. For the model with $M_\star = 0.1863\, M_\odot$, we show the comparison between the observed and the theoretical periods in Table 28.

Considering these results, we may adopt the mentioned model, with $M_\star = 0.1863\, M_\odot$ and $T_{\rm eff} = 8221$ K, which although it is not quite in line with the spectroscopic result for the mass ($M_\star^{\rm (3D)} = 0.149 \pm 0.011\, M_\odot$) and the $T_{\rm eff}$, is a very good period fit (with all the periods associated with $\ell = 1$ g modes), and also has all the periods associated with pulsationally unstable modes.

4. Summary and conclusions

We have presented a detailed asteroseismological study of all the known pulsating ELM WD stars (ELMVs), considering the pulsation spectrum they exhibit and employing the set of evolutionary models of Althaus et al. (2013). This is the fifth paper in a series of works dedicated to pulsating low-mass He-core WDs (including ELMV WDs). The present paper was devoted to performing the first asteroseismological analysis of all the known ELMV stars. For this purpose we employed some asteroseismological tools. One of them is based on the comparison between the observed period spacing of the star under analysis with the average of the period spacings computed on our grid of models. We therefore first tried to determine the observed period spacing for each target star through three independent significance tests. Because the stars under study exhibit few periods, we could only follow this approach for the cases of the stars showing four periods or more, that is, for J1840, J1112, J1518, and J1735. However, for the first two stars we could not find any unambiguous constant period spacing. In the case of J1518 and J1735, on the other hand, we found a clear indication of a constant period spacing at roughly 44 s and 59 s, respectively, from the three significance tests we applied. After comparing these values with the average of the computed period spacings for our grid of models, we found that the resulting stellar masses (greater than $0.4352\, M_\odot$ in both cases) are higher than expected for this type of stars. In the case of J1518, it may be associated with the fact that this star is not pulsating in the asymptotic regime (Córsico & Althaus 2014a). The case of J1735 is more intriguing because this star seems to be in that regime.

Next, we searched for the best-fit model, that is to say, the theoretical model that provides the best match between the individual pulsation periods exhibited by the star and the theoretical pulsation periods. We assessed the function $\chi^2 = \chi^2(M_\star, T_{\rm eff})$ (given by Eq. (2) of Sect. 3.3) for our complete set of model sequences, covering a wide range in effective temperatures ($13\,000 \gtrsim T_{\rm eff} \gtrsim 6000$ K). Because of the multiplicity of solutions, we were forced to employ some external constraints (for instance, the uncertainty in the $T_{\rm eff}$, given by spectroscopy). We assumed that all of the observed periods

correspond to $\ell = 1$ g modes and considered them to compute the quality function for each target star. We also considered the (unlikely) case in which all of the observed periods correspond to $\ell = 2$ g modes. Finally, we considered the case of a mix of $\ell = 1$ and $\ell = 2$ g modes. For the particular case of the star J1112, we performed two different analyses. Since the two shortest periods reported for this star are not confirmed (Hermes et al. 2013b), we first carried out a period fit applied to the subset of the five longest periods exhibited by this star considering they are associated with $\ell = 1$, $\ell = 2$ and a mix of $\ell = 1$ and $\ell = 2$ g modes. Second, for the whole set of seven periods, we explored two possibilities: that all of the observed periods correspond to a mix of g and p modes ($\ell = 1$), and also the case in which the observed periods correspond to radial ($\ell = 0$) and p and g modes ($\ell = 1, 2$). In Table 29 we show a compilation of the mass determinations for the ELMVs both from spectroscopic (other works) and period-fit results (this work). Considering the obtained results, we found that the seismological mass is in good agreement with the spectroscopic determinations for J1840 (in the case of a mix of $\ell = 1, 2$ g modes), J1614 (for the case of $\ell = 1$ g modes), J2228 (for the case of $\ell = 1, 2$ g modes), J1618 (for the case of $\ell = 1, 2$ g modes), and J1735 (for the case of $\ell = 1, 2$ g modes). We consider that there is a good agreement between the seismological and spectroscopic mass when the difference is below the uncertainty of 15%, that is, the typical difference in the mass value derived from independent sets of evolutionary tracks. Then, we conclude that for most of the target stars, the adopted models from the asteroseismological analyses have masses that are in line with the spectroscopic results. At variance with this, for four stars (J1738, J1518, J1112 and J2139) we obtained a higher value of the stellar mass in comparison with the spectroscopic determinations. In particular, gathering together the mass determinations for J1518, we conclude that there is no agreement between the mass given by the spectroscopy ($M_\star^{\rm 1D} = 0.220\, M_\odot$ and $M_\star^{\rm 3D} = 0.197\, M_\odot$), the mass obtained from the comparison between the observed period spacing and the average of the computed period spacings (which is higher than $0.4352\, M_\odot$), and the mass from the adopted asteroseismological model ($M_\star = 0.2707\, M_\odot$). We also mention that although we were able to adopt a seismological model for J1735 whose mass ($M_\star = 0.1612\, M_\odot$) is in line with the spectroscopic determination ($M_\star = 0.142 \pm 0.010\, M_\odot$), we failed to find such an agreement for the mass resulting from the comparison between the observed period spacing and the average of the computed period spacings ($M_\star \gtrsim 0.44\, M_\odot$). Reversing the argument, as this star seems to be in the asymptotic regime, if the value we have obtained for the period spacing of this star were in fact associated with high radial order g modes, it could indicate that the stellar mass is higher than the determined by the spectroscopic and the period-to-period fit analysis, although in that case the star could not be classified as an ELMV WD star. Finally, it is worth mentioning that in general, the pulsation periods corresponding to the asteroseismological models adopted in this work for the analyzed ELMV WDs are pulsationally unstable, according to our nonadiabatic computations. This agreement between the adiabatic and nonadiabatic predictions gives more relevance to our asteroseismological results.

From the results presented in this paper for all the known ELMVs, the power of this approach is evident once again because in most of the cases we were able to constrain the value of the stellar mass. Moreover, when a model has been adopted, we can access additional information, as can be seen in Table 30, which is another advantage of asteroseismology. Taking into account these results, four of the stars we analyzed (J1840, J1518,

Table 29. Stellar masses (in solar units) for all of the studied ELMV WD stars.

Star	Period fit			Spectroscopy	
	$\ell = 1$ (g)	$\ell = 1, 2$ (g)	$\ell = 1, 2(g, p)$ $\ell = 0$ (radial)	(other works) 1D	3D
J1840	0.2389	0.1805	–	0.183^a	0.177^f
J1112	0.3205*	0.2389*	0.1612**	0.179^b	0.169^f
J1518	0.3205	0.2707	–	0.220^b	0.197^f
J1614	0.1762	0.3205	–	0.192^c	0.172^f
J2228	0.1650	0.1554	–	0.152^c	0.142^f
J1738	0.4352	0.4352	–	0.181^d	0.172^f
J1618	0.2019	0.1706	–	0.220^e	0.179^f
J1735	0.3624	0.1612	–	–	0.142^g
J2139	0.1863	–	–	–	0.149^g

Notes. [*] Determined using a subset of the observed periods. [**] Determined using the whole set of the observed periods. [a] Hermes et al. (2012). [b] Hermes et al. (2013b). [c] Hermes et al. (2013a). [d] Kilic et al. (2015). [e] Bell et al. (2015). [f] Determined using the corrections for 3D effects by Tremblay et al. (2015). [g] Bell et al. (2017).

Table 30. Main characteristics of the adopted asteroseismological model for every known ELMV WD.

Star	T_{eff} [K]	$\log(g)$ [cgs]	$M_\star[M_\odot]$	$\log(R_\star/R_\odot)$	$\log(L_\star/L_\odot)$
J1840	9007	6.6156	0.1805	–1.4609	–2.1487
J1112*	9300	6.9215	0.2389	–1.5528	–2.2757
J1518*	9789	7.0956	0.2707	–1.6126	–2.3098
J1614	8862	6.3832	0.1762	–1.3497	–1.9547
J2228	7710	6.1738	0.1554	–1.2725	–2.0409
J1738*	9177	7.6241	0.4352	–1.7746	–2.7447
J1618	9076	6.2403	0.1706	–1.2857	–1.7852
J1735	8075	6.2241	0.1612	–1.2899	–1.9957
J2139*	8221	6.6515	0.1863	–1.4724	–2.3279

Notes. [*] Solution whose mass is in conflict with the spectroscopic results.

J1738, and J2139) are not strictly ELM WD according to our definition previously stated, that is, the progenitors of these stars might have experienced multiple flashes.

In Fig. 16 we show the location of the nine analyzed ELMVs (according to the 3D model-atmosphere parameters) and the corresponding values of T_{eff} and $\log g$ of the asteroseismological models adopted for each star, along with our evolutionary tracks of low-mass He-core WDs and the instability domain of $\ell = 1$ g modes computed by Córsico & Althaus (2016). As we mentioned, for five stars we found good agreement between the seismological mass and the spectroscopic one, and for the remaining four stars, the agreement is poor. In addition, Fig. 16 demonstrates that for eight out of nine stars we analyzed, the asteroseismological models are more massive (i.e., they are characterized by higher gravities) in comparison with the spectroscopy results. This systematic trend is also found in the case (not shown) in which the T_{eff} and $\log(g)$ values derived from calculations of 1D atmospheres are adopted. This trend could be related, in part, to the fact that we did not consider low-mass He-core WD models characterized by outer H envelopes thinner than those predicted by the complete binary evolutionary history of the progenitor stars. Alternatively, it could be an indication that the spectroscopic determinations of $\log g$ and T_{eff} in this class of stars were not correct.

In this paper, we have considered low-mass He-core WDs coming from solar metallicity progenitors, typical of the population of the Galactic disk. The threshold in the stellar mass value below which CNO flashes on the early WD cooling branch are not expected to occur is $\sim 0.18 \ M_\odot$. If we had adopted progenitors with lower metallicities, representative of the population of the Galactic halo, the threshold mass limit should be higher (see Serenelli et al. 2002; Nelson et al. 2004; Istrate et al. 2016b). The H envelope of the low-mass WDs should also be thicker than those obtained in Althaus et al. (2013; e.g., Istrate et al. 2016b). This means that when we assume that some of the ELMVs studied in this work are objects of the Galactic halo, the asteroseismological analysis should be based on evolutionary models coming from low-metallicity progenitors, and therefore the characteristics of the asteroseismological models for each analyzed star could be different to those obtained in this work.

We here considered low-mass He-core WD models characterized by thick outer H envelopes, consistent with the previous evolution. We are well aware that there are strong uncertainties about the precise value of the thickness of this envelope. We cannot discard that WD models with H envelopes thinner than those characterizing our set of models could result from binary evolution computations that assume different angular-momentum loss prescriptions due to mass loss, different initial mass-ratio, etc., than that adopted in Althaus et al. (2013; see the detailed works by Istrate 2015; Istrate et al. 2016b). Asteroseismological analyses considering low-mass He-core WD models characterized by thinner outer H envelopes will be the core feature of a future work.

References

Althaus, L. G., Serenelli, A. M., Panei, J. A., et al. 2005, A&A, 435, 631
Althaus, L. G., Panei, J. A., Romero, A. D., et al. 2009, A&A, 502, 207
Althaus, L. G., Córsico, A. H., Isern, J., & García-Berro, E. 2010, A&ARv, 18, 471
Althaus, L. G., Miller Bertolami, M. M., & Córsico, A. H. 2013, A&A, 557, A19
Althaus, L. G., Camisassa, M. E., Miller Bertolami, M. M., Córsico, A. H., & García-Berro, E. 2015, A&A, 576, A9
Bell, K. J., Kepler, S. O., Montgomery, M. H., et al. 2015, in 19th European Workshop on White Dwarfs, eds. P. Dufour, P. Bergeron, & G. Fontaine, ASP Conf. Ser., 493, 217
Bell, K. J., Gianninas, A., Hermes, J. J., et al. 2017, ApJ, 835, 180
Bischoff-Kim, A., Montgomery, M. H., & Winget, D. E. 2008, ApJ, 675, 1505
Bognár, Z., Paparó, M., Córsico, A. H., Kepler, S. O., & Győrffy, Á. 2014, A&A, 570, A116
Bognár, Z., Paparó, M., Molnár, L., et al. 2016, MNRAS, 461, 4059
Bradley, P. A. 1998, ApJS, 116, 307
Bradley, P. A. 2001, ApJ, 552, 326
Brassard, P., Fontaine, G., Wesemael, F., Kawaler, S. D., & Tassoul, M. 1991, ApJ, 367, 601
Brickhill, A. J. 1991, MNRAS, 251, 673
Brown, W. R., Kilic, M., Allende Prieto, C., & Kenyon, S. J. 2010, ApJ, 723, 1072
Brown, W. R., Kilic, M., Allende Prieto, C., & Kenyon, S. J. 2012, ApJ, 744, 142
Brown, W. R., Kilic, M., Allende Prieto, C., Gianninas, A., & Kenyon, S. J. 2013, ApJ, 769, 66
Brown, W. R., Gianninas, A., Kilic, M., Kenyon, S. J., & Allende Prieto, C. 2016, ApJ, 818, 155
Brown, W. R., Kilic, M., & Gianninas, A. 2017, ApJ, 839, 23
Burgers, J. M. 1969, Flow Equations for Composite Gases (New York: Academic Press)
Calcaferro, L. M., Córsico, A. H., & Althaus, L. G. 2016, A&A, 589, A40
Calcaferro, L. M., Córsico, A. H., & Althaus, L. G. 2017, A&A, 600, A73
Cassisi, S., Potekhin, A. Y., Pietrinferni, A., Catelan, M., & Salaris, M. 2007, ApJ, 661, 1094
Castanheira, B. G., & Kepler, S. O. 2008, MNRAS, 385, 430
Castanheira, B. G., & Kepler, S. O. 2009, MNRAS, 396, 1709
Córsico, A. H., & Althaus, L. G. 2006, A&A, 454, 863
Córsico, A. H., & Althaus, L. G. 2014a, A&A, 569, A106
Córsico, A. H., & Althaus, L. G. 2014b, ApJ, 793, L17
Córsico, A. H., & Althaus, L. G. 2016, A&A, 585, A1
Córsico, A. H., Althaus, L. G., & Miller Bertolami, M. M. 2006, A&A, 458, 259
Córsico, A. H., Althaus, L. G., Miller Bertolami, M. M., & Werner, K. 2007a, A&A, 461, 1095
Córsico, A. H., Miller Bertolami, M. M., Althaus, L. G., Vauclair, G., & Werner, K. 2007b, A&A, 475, 619
Córsico, A. H., Althaus, L. G., Kepler, S. O., Costa, J. E. S., & Miller Bertolami, M. M. 2008, A&A, 478, 869
Córsico, A. H., Althaus, L. G., Miller Bertolami, M. M., & García-Berro, E. 2009, A&A, 499, 257
Córsico, A. H., Althaus, L. G., Miller Bertolami, M. M., & Bischoff-Kim, A. 2012a, A&A, 541, A42
Córsico, A. H., Romero, A. D., Althaus, L. G., & Hermes, J. J. 2012b, A&A, 547, A96
Córsico, A. H., Althaus, L. G., Serenelli, A. M., et al. 2016, A&A, 588, A74
Corti, M. A., Kanaan, A., Córsico, A. H., et al. 2016, A&A, 587, L5
Dziembowski, W. A. 1971, Acta Astron., 21, 289

Dziembowski, W. 1977, Acta Astron., 27, 203
Fontaine, G., & Brassard, P. 2008, PASP, 120, 1043
Fontaine, G., Istrate, A., Gianninas, A., Brassard, P., & Van Grootel, V. 2017, in 20th European White Dwarf Workshop, eds. P.-E. Tremblay, B. Gaensicke, & T. Marsh, ASP Conf. Ser., 509, 347
Giammichele, N., Fontaine, G., Brassard, P., & Charpinet, S. 2016, ApJS, 223, 10
Giammichele, N., Charpinet, S., Brassard, P., & Fontaine, G. 2017a, A&A, 598, A109
Giammichele, N., Charpinet, S., Fontaine, G., & Brassard, P. 2017b, ApJ, 834, 136
Gianninas, A., Dufour, P., Kilic, M., et al. 2014a, ApJ, 794, 35
Gianninas, A., Hermes, J. J., Brown, W. R., et al. 2014b, ApJ, 781, 104
Gianninas, A., Kilic, M., Brown, W. R., Canton, P., & Kenyon, S. J. 2015, ApJ, 812, 167
Gianninas, A., Curd, B., Fontaine, G., Brown, W. R., & Kilic, M. 2016, ApJ, 822, L27
Haft, M., Raffelt, G., & Weiss, A. 1994, ApJ, 425, 222
Handler, G., Pikall, H., O'Donoghue, D., et al. 1997, MNRAS, 286, 303
Hermes, J. J., Montgomery, M. H., Winget, D. E., et al. 2012, ApJ, 750, L28
Hermes, J. J., Montgomery, M. H., Gianninas, A., et al. 2013a, MNRAS, 436, 3573
Hermes, J. J., Montgomery, M. H., Winget, D. E., et al. 2013b, ApJ, 765, 102
Hermes, J. J., Gänsicke, B. T., Koester, D., et al. 2014, MNRAS, 444, 1674
Iglesias, C. A., & Rogers, F. J. 1996, ApJ, 464, 943
Istrate, A. G. 2015, in 19th European Workshop on White Dwarfs, eds. P. Dufour, P. Bergeron, & G. Fontaine, ASP Conf. Ser., 493, 487
Istrate, A. G., Fontaine, G., Gianninas, A., et al. 2016a, A&A, 595, L12
Istrate, A. G., Marchant, P., Tauris, T. M., et al. 2016b, A&A, 595, A35
Itoh, N., Hayashi, H., Nishikawa, A., & Kohyama, Y. 1996, ApJS, 102, 411
Kawaler, S. D. 1988, in Advances in Helio- and Asteroseismology, eds. J. Christensen-Dalsgaard, & S. Frandsen, IAU Symp., 123, 329
Kepler, S. O., Pelisoli, I., Peçanha, V., et al. 2012, ApJ, 757, 177
Kepler, S. O., Fraga, L., Winget, D. E., et al. 2014, MNRAS, 442, 2278
Kilic, M., Brown, W. R., Allende Prieto, C., et al. 2011, ApJ, 727, 3
Kilic, M., Brown, W. R., Allende Prieto, C., et al. 2012, ApJ, 751, 141
Kilic, M., Hermes, J. J., Gianninas, A., & Brown, W. R. 2015, MNRAS, 446, L26
Koester, D., Voss, B., Napiwotzki, R., et al. 2009, A&A, 505, 441
Magni, G., & Mazzitelli, I. 1979, A&A, 72, 134
Maxted, P. F. L., Anderson, D. R., Burleigh, M. R., et al. 2011, MNRAS, 418, 1156
Maxted, P. F. L., Serenelli, A. M., Miglio, A., et al. 2013, Nature, 498, 463
Maxted, P. F. L., Serenelli, A. M., Marsh, T. R., et al. 2014, MNRAS, 444, 208
Nelson, L. A., Dubeau, E., & MacCannell, K. A. 2004, ApJ, 616, 1124
O'Donoghue, D. 1994, MNRAS, 270, 222
Paparó, M., Bognár, Z., Plachy, E., Molnár, L., & Bradley, P. A. 2013, MNRAS, 432, 598
Pech, D., & Vauclair, G. 2006, A&A, 453, 219
Pech, D., Vauclair, G., & Dolez, N. 2006, A&A, 446, 223
Romero, A. D., Córsico, A. H., Althaus, L. G., et al. 2012, MNRAS, 420, 1462
Romero, A. D., Kepler, S. O., Córsico, A. H., Althaus, L. G., & Fraga, L. 2013, ApJ, 779, 58
Saio, H., Winget, D. E., & Robinson, E. L. 1983, ApJ, 265, 982
Serenelli, A. M., Althaus, L. G., Rohrmann, R. D., & Benvenuto, O. G. 2002, MNRAS, 337, 1091
Steinfadt, J. D. R., Bildsten, L., & Arras, P. 2010, ApJ, 718, 441
Tassoul, M. 1980, ApJS, 43, 469
Tassoul, M., Fontaine, G., & Winget, D. E. 1990, ApJS, 72, 335
Tremblay, P.-E., Gianninas, A., Kilic, M., et al. 2015, ApJ, 809, 148
Unno, W., Osaki, Y., Ando, H., Saio, H., & Shibahashi, H. 1989, Nonradial oscillations of stars, 2nd edn. (Tokyo: University of Tokyo Press)
Van Grootel, V., Fontaine, G., Brassard, P., & Dupret, M.-A. 2013, ApJ, 762, 57
Winget, D. E., & Kepler, S. O. 2008, ARA&A, 46, 157
Zhang, X. B., Fu, J. N., Li, Y., Ren, A. B., & Luo, C. Q. 2016, ApJ, 821, L32